Thermal and exergy analysis of the use of the lens in parabolic trough

Pezhman ghareghani[a], Sadegh Alikhani[a], Iman Khatami[a], Mohammad Yaghoub Abdollahzadeh Jamalabadi[b]*

Chabahar Maritime University, Chabahar, Iran[a]
Department of Mechanical, Robotics and Energy Engineering, Dongguk University, Seoul 04620, Korea[b]*

Abstract

The aim of current study, is looking for a new way to increase the efficiency of the solar collector parabolic trough analytical and experimentally. To do a collector through is produced and equiped with 23 lenses located above the absorber tube in a row. The use of the lens increase the efficiency of Parabolic trough collector up to 14 percent. The system analysed theorically and evaluates by first and second law of thermodynamics. For the estimation of solar radiation the two methods of maximum probability and Prescott's angstrom methods is used, and compared with the data of the pyrometer device (radiation gauge). By the statistical criteria, the Angstrom method is more accurate compared to the maximum probability. Various components of heat transfer is analyzed through the system evolution versus time. The results show that the maximum exergy efficiency of the system was about 52 percent. As well the use of lens enhance the exergy efficiency of the system.

Keywords: Parabolic trough solar collector Optical lens Angstrom method numerical simulation

Introduction

The use of these renewable energies results in very small quantities and, in some cases, no greenhouse gas emissions, solar energy harvesting is one of the fastest-growing fuels in the world. Since the use of solar energy in order to provide hot water, heating and cooling of spaces in recent decades has been very much considered [1]. Solar energy has been known and used for centuries. The use of solar energy dates back to the time of history [2]. During the pottery period, clerics used temples to shine the sun's bright sunlight to illuminate the temple. One of the uses of solar energy is the Greek scientist, Archimedes, who burned Roman ships by burning light reflectors with small mirrors with thermal energy from the sun. In Iran other than the northern regions of the country, the average annual sunshine is more than 300, which is very significant. The amount of solar radiation in Iran is estimated to be between 1800 and 2200 KWh/m^2, which is, of course, above the global average citefan2018heat, freedman2018analysis. This amount of energy is more than 4,000 times the total energy consumed in the country. Fig. 1 shows a parabolic trough at a plant near Harper Lake. The benefits of solar energy include renewable energy, the abundance of solar energy: sustainability, cleanliness, easy access, affordability, diversity of use, multiple use, quietness, government support and low maintenance. The disadvantages of solar energy include the cost of initial setup, the need for sunlight, the cost of storing energy and the need for sufficient space for installation [2].

The parabolic trough technology consists of a linear parabolic reflector that concentrates light onto a receiver pipe with an absorber surface positioned through the reflectors focal line [3, 4, 5]. Fig. 2 shows a diagram of a parabolic trough solar farm and an end view of how a parabolic collector focuses sunlight onto its focal point. The absorber surface of a receiver is a coated metal absorber encovered by a glass envelope in an annulus geometry. There are various methods to improve the efficiency of the parabolic trough technology consists of a linear parabolic reflector. One of newest approach is the use of nano-particle in convective fluid [6, 7]. Those particles can directly absorb the solar radiation. The use of Nanoparticles in solar energy transfer has been incestigated in many applications [8, 9, 10, 11, 12, 13, 14, 15, 16, 17, 18]. In some references the dircet absorbtion in Nanoparticles were studied [19, 20, 21, 22, 23, 24, 25, 26, 27, 4]. Another way would be use of optical lens [28, 29, 30, 31, 32, 33, 34, 35, 36, 37, 38, 39, 40, 41, 42, 43, 44, 45, 46]. The basics of the solar collector is investigated by Incropera [30]. The sun

rays travel through the transparent glass and reach the absorber at inner tube. Since, the strengthen the optical length (absorption coefficient×diameter of the tube) requires high value of the absorption (following the shape of solar spectrum) to satisfy the high energy absorption [14]. The thermal radiation of the absorber tube is not dissipated completely to the environment as the transparency of glass for the long-wavelength thermal emission is in the mid-infrared spectral region [30]. In this study analytical and experimental investigation using lens in a linear linear solar cell and studying heat transfer and radiation estimation are performed. Fig. 3 shows the experimental setup used in current study. First the statistical analysis of solar radiation for the city of Karaj is performed by the use of Angstrom method . Then the performance analysis of the optical lens assisted parabolic trough solar collector is performed numerically.

1 Mathematical model

Fig. 4 shows the cross section of device. Characteristics of the collector in the East-West direction exposed to the south. Here a theoretical model of a linear parabolic trough solar collector is presented in Table 1.

As presented in Table 1, the length of the collector does not seem to be equal to the width (same as in Fig.1). The optical and thermal properties presented in Table 1 measured. The absorber tube made of a specific graphite material. Since its thermal conductivity is higher than the materials similar to stainless steel (which thermal conductivity is about 16 W/m K). In the most references the convection inside the absorber tube calculated by the laminar regime correlation ($h_{htf} = \mathrm{Nu}_{htf}\frac{k_{htf}}{D_{ia}}$,$\mathrm{Nu}_{htf} = 4.36$) or turbulent regime correlation ($\mathrm{Nu} = \frac{f/8(\mathrm{Re}_{htf}-1000)\,\mathrm{Pr}_{htf}}{1+12.7\sqrt{f/8}(\mathrm{Pr}_{htf}^{2/3}-1)}\left(\frac{\mathrm{Pr}_{htf}}{\mathrm{Pr}_{ia}}\right)^{0.11}$,$f = (0.79\mathrm{InRe}_{htf} - 1.64)^{-2}$). The thermal equilibrium in different parts of the linear parabolic collector is as follows:

1. Thermal balance at the inner surface of the receiver tube
2. Thermal balance on the receiver tube surface
3. The thermal equilibrium at the inner surface of the glass cover
4. Thermal balance on the surface of the glass cover
5. thermal dissipation at the outer surface of the glass cover.

$$Q_{irradiance\ solar} = Q_{loss} + Q_{radiation,sky} + Q_{support,bellow} + Q_{convection,env} + Q_{absorber\to glass}, \tag{1}$$

where $Q_{absorber\to glass} = A_{ro}\cdot\sigma\cdot\frac{T_r^4-T_c^4}{\frac{1}{r}+\frac{1-c}{c}\cdot\frac{A_{ri}}{A_{co}}}$, $Q_{radiation,sky} = A_{co}\cdot\sigma\cdot{}_c\cdot\left(T_c^4 - T_{sky}^4\right)$, $Q_{convection,env} = A_{co}\cdot h_{out}\cdot(T_c - T_{am})$,and $h_{out} = 4\cdot V_{wind}^{0.58}\cdot D_{co}^{-0.42}$. The efficiency of the performance of the system can be estimated from

$$\eta_{thermal} = \frac{Q_u}{Q_{sun}\times A_a} \tag{2}$$

where the Q_{sun} is the direct beam solar irradiation,A_a is the solar area or the total collector aperture which is the product of the width and the length $(W\cdot L)$, the useful heat absorbed in the fluid Q_u is calculated using the energy balance on the fluid volume $(\dot{m}\cdot c_p\cdot(T_{out}-T_{in}) = A_{ro}\cdot h\cdot\left(T_r - \frac{T_{in}+T_{out}}{2}\right))$, and according to the DittusBoelter model $h = \frac{0.023\cdot Re^{0.8}\cdot Pr^{0.4}\cdot k}{D_{ri}}$. In the above equation the maximum optical efficiency is considered. If the solar irradiation incident angle $\theta = Arccos\left(\sqrt{\cos^2(\theta_z)+\cos^2(\delta)\cdot\sin^2(\omega)}\right)$ differs from zero incident angle, the optical efficiency is a function of the zenith solar angle θ_z, the solar declination angle δ and the solar hour angle ω, absorber absorbance α, the cover transmittance τ, the intercept factor γ and the total reflectance ρ_{tot} , collector focal distance f ,and geometric parameters :

$$\eta_{optic}(\theta) = \gamma\tau\alpha\rho_{tot}\left(\cos(\theta) - \frac{f}{L}\cdot\left(1+\frac{W^2}{48\cdot f^2}\right)\cdot sin(\theta)\right) \tag{3}$$

The thermal losses of the solar collector is expressed as below, using the thermal loss coefficient U_L, the mean absorber temperature T_r and the absorber outer surface $(A_{ro} = \pi\cdot D_{ro}\cdot L)$:

$$Q_{loss} = A_{ro}\cdot U_L\cdot(T_r - T_{am}) \tag{4}$$

in some references for the pumping power ($W_p = \frac{\dot{m}\cdot 0.092\cdot Re^{-0.2}\cdot L\cdot u^2}{D_{ri}}$) is also considered in efficiency calculation but here it is neglected. Although the pumping power affect the useful exergy production ($Q_u - m\cdot c_p\cdot T_o\cdot \ln\left[\frac{T_{out}}{T_{in}}\right] - \frac{m\cdot T_o\cdot \Delta P}{\rho\cdot T_{fm}}$) but the exergy flow of the solar irradiation can not exceed the 93 percent of the solar irradiation ($E_{solar} = Q_{sun}\cdot \left[1 - \frac{4}{3}\cdot\frac{T_{amb}}{T_{sun}} + \frac{1}{3}\cdot\left(\frac{T_{amb}}{T_{sun}}\right)^4\right]$).

In 1924, Angstrom proposed a relationship for estimating solar radiation, which is a linear relationship based on the sunshine and the amount of radiation produced, so that by the Angstrom method it is easy to calculate the amount of solar energy that has reached the surface, like as below

$$q_{surf} = q_{atm}\left(a + b\frac{n}{N}\right) \tag{5}$$

In this case, q_{surf} is the amount of energy spun daily in a unit area, and q_{atm} is the amount of solar energy emitted per unit area at the top of the atmosphere, n is the average daily sunshine, N is the average number of sunshine hours per day, a, b, the coefficients Angersmoum, depending on factors such as latitude, weather conditions, temperature, etc. Motennis proposed that for areas with very dry climates, and where radiation measurement devices are not available at these locations, the Angstrom coefficients are 0.25 and 0.5 (the average of Iran is 0.251 and 0.46). As well The maximum possible model propose a relationship for estimating solar radiation. In this model, a quadratic equation is used to estimate the radiation energy, which is the daily sunshine / day ratio. In the max possibility approach the following equation is used:

$$q_{surf} = q_{atm}\left(C_1 + C_2\frac{n}{N} + C_3(\frac{n}{N})^2\right) \tag{6}$$

In convergent lenses, when the sun's rays collide with the lens surface, the lens focuses the rays at the focal point. In this analytical and laboratory study, we want to reflect the sun's radiation on the collector tube by examining the effects of the lens.

2 Results and discussion

2.1 Experimental rig

In this chapter, the equipment and instruments used during the test and then the data obtained from the test are examined. The aim of this experiment was to optimize the linear parabolic cluster collector at the Materials and Energy Research Center of Meshkin-e-Dasht, Karaj, Alborz province. To optimize and improve the performance of the solar collector system, the convergent lens (magnifier) along the focal length was installed on the collector, which significantly increased the temperature. The output data of the temperature and wind speed were measured by a digital thermometer and an anemometer. The amount of solar energy and daytime sunshine (daytime) with data channel channels were obtained by the CM22 Pyrmaneter device and the BD300 daylight sensing device found on the solar energy site of the Materials and Energy Research Center The supplies and equipment used during the test are as follows, which will be followed in more detail on how they work and how to test and output data from them.

1. linear parabolic solar collector
2. Wind gauge
3. 23 Convertible lens
4. pyranometer (model Kipp Zonen)
5. Daylight Sensor (Model BD300)
6. Rod bars
7. Thermometer

The linear parabolic collector method is that the fluid flows from the initial part of the collector through the tube into the absorbent tube, the radiation of the sun is shifted through the reflective plate to the surface of the absorbent

tube and the fluid is heated inside it and from the part The ends of the collector are removed. The test was carried out at the Mashinkin Research Institute for Materials and Energy of Karaj, Alborz province, every half hour. To optimize and improve the performance of the solar collector system, linear parabolic gyrations converged lenses along the focal length, with a significant increase in temperature. 23 lenses of 75 mm diameter, as shown in Figure 3-a, were mounted in a row 23 in the upper part of the absorber tube at the focal length of the pipe surface by a metal base at the end of which a pipe clamp was placed. By this lens, we focused the sun's radiation in the focal length of the lens on the tube as a point in order to increase the temperature of the surface of the absorbent tube. In this test, all parameters were checked for everyday without lens and bundle with a constant flow rate for each day of the experiment every half hour and achieved the desired results. All temperatures are Kelvin. We recorded parameters such as ambient temperature and inlet fluid temperature, and the outlet fluid and absorbent tube surface and glass cover, by a digital memory thermometer during testing and wind speed by an anemometer at each instant of the test. The pyranometers are used to measure the downward and upward ($i.e$ reflected) solar irradiance through a horizontal surface (in W/m^2).

The flow of the inlet fluid by Human beings in a given volume at different times for each day, calculating the solar energy and solar energy from the CM22 device's perinometer devices with 2 channel data analyzers and the BD300's daytime lighting sensor, with the 4-channel data analyst in The solar energy site of the Institute of Materials and Energy was located. According to the obtained parameters, heat transfer rate and efficiency can be calculated. Due to limitations in the research laboratory and the current costs, the water was used as an operating fluid in this experiment.

Cost implications of including the lenses in the system (see Fig. 3) is 20 USD where compared to the price of the conventional systems is less than 10 percent. The schematic of layers are presented in Fig. 4. Fig. 4 presents the geometry without the rays incident on the collector and how they are reflected onto the receiver.

2.2 Effects of the radiation model

Sun irradiance Q_sun at the collector location is an important parameter for the thermal performance of solar collector by influencing the local heat input to the system. Fig. 5 presents the input radiation and calculation of radiation with two methods numerically and experimentally. In this section, effects of the radiation model coefficient are investigated for the various working days. The configuration of the collector is the same for all working days. The sun angles versus time is plotted in Fig. 6. The measured and calculated heat flux based on the sun angles is shown in Fig. 7. The data is measured and calculated every one hour which is a typical changing time. It can be seen from Fig. 7(a-e) that the irradiance Q_sun keeps increasing with increasing time till the noon and decreasing after that. As well the average of daily measured solar radiation is compared in Table 3 and the figure Fig. 7. Measuring instruments specifications is specified in Table 4. With regard to the measured radiation, the radiometric or radiometric stations with a correlation coefficient of r = 0.91 the following equation are obtained:

$$q_{surf} = q_{atm}\left(0.1088 + 0.9749\frac{n}{N} - 0.4421(\frac{n}{N})^2\right) \tag{7}$$

Fig. 5 shows the numerical and experimental calculation of the solar radiation. Error of calculation methods is presented in Table 2 in detail. The detail of daily calculation of solar radiation is given in Fig. 6. Fig. 6 shows the sun angles vs time on 10/7/2018. The resulted figure which calculates the Radiation vs time on 15/7/2018 is plotted in Fig. 7. The measured values of the temperature in various position of the device is plotted in Fig. 8. It can be also seen from Fig. 8 that at the same conditions, the lens supported solar thermal collector performs better than the usual solar thermal collector, especially for initial times of the day. It is important to note that the usual solar thermal collector with near doubled values of the efficiency at the 11.5 o'clock (i.e., both collectors have the same conditions) can perform the same as the lens supported solar thermal collector. The main reason is that the emissivity of the inner tube surface for the casual solar thermal collector (i.e., half glass surface and half metallic coating) help to absorb more radiation of solar thermal collector, leading to lower radiation loss. Another reason is that incident flux is doubled for the solar thermal collector, the heat source as well as the resulting temperature distribution will be not as uniform as the usual solar thermal collector at the corresponding values (i.e., similar conditions), leading to locally high temperature on the inner tube surface thus more heat loss [refer to Fig. 8. The absorbed heat to the system versus time is plotted Fig. 9. The increasing solar radiation rate gets slower with increasing time and becomes maximum near noon. Note that angstrom method has a better predictions for solar radiation. Similarly, the collector thermal efficiency η also increases with the increase of time at first and then starts to decrease when exceeding noon

time. The reason is that, at lower value of time, the increase of solar radiation rate causes more solar energy to be absorbed in the pipe. However, as times goes on, the contribution by increasing q_{sun} becomes limited while the heat loss keeps increasing. The efficiency of the system with and without the lens versus time is plotted Fig. 10. Here, Q_{loss} is defined as the total heat loss (i.e., both thermal radiation and heat convection from the glass outer surface). The increased heat loss to the surrounding eventually leads to the decrease in the collector efficiency at those conditions. In other words, the lens supported solar thermal collector requires lower value of liquid mass flow rate for the same level of the thermal performance, which is beneficial for avoiding high pumping powers and maintaining stable operation. For initial times of the day, the advantage of the lens supported solar thermal collector becomes minimal because the absorption of the solar radiation is already high enough for the usual solar thermal collector. Nevertheless, due to the low emissivity of the metallic reflective coating, the lens supported solar thermal collector still exhibits the thermal efficiency which is slightly higher than the value of the usual solar thermal collector.

2.3 Effects of the wind velocity

The numerical solution procedure in this study is based on the solution of energy balance (See Eq. (1)) by using correlation for each part independently. In this section, effects of the wind velocity is investigated, and comparisons are made for the solar thermal collector and the lens supported solar thermal collector. For fair comparison, we set conditions to be constant for different values of wind velocity for solar thermal collector. Fig. 11 shows the device used for the velocity measurement and the measured values are plotted in Fig. 12. Figures 13(a) and 13(b) show that η_{th} of all the three collectors decreases with increasing V_{wind} due to nearly constant Q_sun value as well as increasing heat loss. Besides, the decrease rate of η_{th} for solar thermal collector is much slower than the lens supported solar thermal collector owing to their much lower heat loss, which arises from the fact that the forced convection of the glass tube increased. Figure 13(a) suggests that the solar thermal collector are more suitable for collectors with lens than the usual. For instance, the lens supported solar thermal collector performs better than the solar thermal collector when $V_{wind} > 2\frac{m}{s}$. It should also be noted that for the given condition, the lens supported solar thermal collector require smaller Q_{sun} (i.e., lower radiation) with increasing V_{wind}, which is beneficial for avoiding heat loss and maintaining stable collector performance. Because h_{conv} is inversely proportional to V_{wind} when Q_{conv} becomes lager. In principle, larger η_{th} and smaller Q_{sun} are desirable; thus, there exists an optimal value of D_{glass} where the solar thermal collector can gain a reasonably high η_{th} at a sufficiently low V_{wind} for stable operation. For instance, the lens supported solar thermal collector with $V_{wind} = 2\frac{m}{s}$ in Fig. 13(a) has $\eta = 0.538$, which is more advantageous than the one obtaining slightly higher $\eta = 0.543$ but with much liquid flow rate value. Now the value of V_{wind} increases from 0.1 to 4.5 in Figs. 13(c) and 13(d), along with the same condition as in Figs. 13(a) and 13(b) for comparison. We can see that the solar thermal collector with lens show higher η_{th} values. This is mainly due to the increased convection heat losses.

2.4 Effects of the flow rate

The effect of flow rate on the collector performance is investigated here in the range from 0.02 to 0.3 kg/s with the corresponding $Re_D = 100 \sim 300$. The mass flow rates are 0.016, 0.01, 0.008, 0.005, and 0.006 kg/s. Performance of two collectors including the solar thermal collector with and without lens are compared in Fig. 13. It can be seen from Fig. 13(a) that as the flow rate $\dot{m}$ increases, the collector thermal efficiency η_{th} increases but its increasing rate slows down gradually. This can be explained based on the following two perspectives. First, recall that η_{th} is determined by energy equation and any change in η_{th} is due to the variation of the three parameters, i.e., $\dot{m}$, ΔT (or $\bar{T}_{out} - T_0$) and c_p. With the increase of $\dot{m}$, ΔT first decreases significantly and then the decrease rate becomes slower, as shown in Fig. 13(b). In addition, c_p also decreases with slower decreasing rate as $\dot{m}$ increases because it has approximately linear relation with the average temperature T_m (i.e., $\frac{T_0+\bar{T}_{out}}{2} = T_0 + \Delta T/2$), as noted from Fig. 13(c). Although both ΔT and c_p decrease with increasing $\dot{m}$, increase in $\dot{m}$ leads to the increasing η_{th} at initial stage. To be more specific, when $\dot{m} < 0.01$ kg/s, the decreasing effects of ΔT and c_p are less than the increasing effect of $\dot{m}$, so there is an obvious increase for η. For instance, for the case of lens used collector, when $\dot{m}$ changes from 0.002 to 0.01 kg/s (increased to 250%), ΔT decreases from 266.46 to 125.79 K (decreased to 47%) and the corresponding decrease of c_p is decreased from 4177 to 4188 J/kg-K (decreased to 0.25%), resulting in η_{th} increased to ≈ 0.41. For both collector, when $\dot{m} > 0.01$ kg/s, the decreasing effect of ΔT and c_p become nearly offset to the increasing effect of $\dot{m}$, leading to almost constant η_{th}.

The second reason for describing the change of efficiency (η_{th}) with mass flow rate ($\dot{m}$) is through the first law of thermodynamics analysis. Since mass flow rate ($\dot{m}$) does not affect the area of the device (A_m), the absorbed

solar energy (Q_{abs}) in solar thermal collector is independent of mass flow rate ($\dot{m}$). As a result, the change of η_{th} is a function of the heat loss change (Q_{loss}); that is, the higher heat loss (Q_{loss}) is, the lower efficiency (η_{th}) will be. This is easily recognized in Figs. 13(a) and 13(d). Furthermore, the effect of mass flow rate ($\dot{m}$) on heat loss (Q_{loss}) can be explained as follows. At small values of mass flow rate ($\dot{m}$), the fluid spends much time in the solar collector receiver tube; since, higher temperature difference (ΔT) can be obtained as in Fig. 5(b). The higher temperature difference (ΔT) in turn cause the higher values of temperature on the solar collector receiver surface and as a result more heat loss (Q_{loss}) is occurred. When the value of the mass flow rate ($\dot{m}$) increases, the corresponding value of the temperature difference (ΔT) decreases, and so does the heat loss value (Q_{loss}). The trend of the value of the heat loss (Q_{loss}) is actually very similar to that of the value of the temperature difference (ΔT) for the solar thermal collector. While for the solar thermal collector, heat loss (Q_{loss}) is much lower than that of the lens supported solar thermal collector as the temperature on the inner tube surface is much lower than that of the solar thermal collector owing to the absorption of the solar radiation on the metallic pipe surface and heat loss on the glass tube.

It is also worthy to noted that efficiency (η_{th}) of the lens supported solar thermal collector is higher than the solar thermal collector without the lens for all values of fluid mass flow rate ($\dot{m}$). This is because when fluid mass flow rate ($\dot{m}$) increased for all the collectors, leading to much less heat loss, especially for the usual solar thermal collector. Since, the usual solar thermal collector are more desirable for low flow rate operation conditions (e.g., $\dot{m} < 0.01$ kg/s) while the lens supported solar thermal collector works better for higher flow rate conditions (e.g., $\dot{m} > 0.01$ kg/s).

2.5 Effects of the inlet temperature

In this section, effects of the inlet temperature on the thermal efficiency of lens supported solar thermal collector and common solar thermal collector (refer to Fig. 2) are studied and compared. First of all,it is worthy to note that as seen from Fig. 13(a) , the collector thermal efficiency η_{th} of all configurations decreases with increasing inlet temperature because of the increasing heat loss [see Fig. 13(b)]. Secondly, Fig. 13(a) also suggests that the best-performance configuration is the lens supported solar thermal collector and this fact is not depends on the inlet temperature (T_{in}). When inlet temperature (T_{in}) is in the range of $10 < T_0 < 30^oC$, for instance, the η_{th} for the lens supported solar thermal collector are higher than the usual solar thermal collector due to the high received heat flux from the sun at lens supported solar thermal collector. Interestingly, the solar thermal collector without the lens performs better than the corresponding lens supported solar thermal collector in the loss of the heat in device. This indicates that the solar thermal collector without the lens become more advantageous than the solar thermal collector with the lens at low temperature owing to their lower heat loss. In other words, at lower temperature applications, improving the solar weighted absorption coefficient by adding the lens is more crucial than decreasing the convection heat loss. When inlet temperature (T_{in}) increases, however, the solar thermal collector with the lens outperform the corresponding solar thermal collector without the lens. It is worth mention that η_{th} of the olar thermal collector with the lens is very close to that of the solar thermal collector without the lens when inlet temperature (T_{in}) is high.

2.6 Heat balance calculations

Fig. 14 shows the viscosity versus time. As shown by increase of time the viscosity decrease as temperature increase. As viscosity is a fluid's resistance to shear stress the Fig. 14 reveals that as times goes on the shear stress decreased. Since the needed pumping power decreased around 30 percent. Moreover, when the fluid viscosity decrease the significance of buoyancy driving force increases by 30 percent. When the significance of buoyancy effects increase it causes a more unevenly distributed fluid flow through the absorber tubes. Substantial viscosity variation with temperature can be exploited in solar collector designs. Through the properties of solar collector fluid, the same trend is seen in Fig. 15. As shown by increase of time, the density decrease as temperature increase. Density can change drastically for some fluids as they heat up but here the change is less than 1 percent and the effect on the performance of the collector is negligible. The Reynolds number is a vital dimensionless amount in liquid mechanics used to help foresee stream designs in various liquid stream circumstances. At low Reynolds numbers, streams will in general be ruled by laminar (sheet-like) stream, while at high Reynolds numbers choppiness results from contrasts in the liquid's speed and bearing, which may at times cross or even move counter to the general heading of the stream (whirlpool ebbs and flows). These swirl flows start to stir the stream, spending vitality all the while, which for fluids builds the odds of cavitation. Calculation of Reynolds number in Fig. 16 is a good representative of regime governs the fluid motion. It should be mentioned that the Reynolds number values indicated in the Fig. 16 is the calculated values at the inlet flow which is larger than the Reynolds number of flow in the outlet where the flow is developed. From the Fig. 16, it

can be seen that the flow rate through the tube tends to increase as time goes on. When the inlet flow rate increases, the flow distribution gets worse. In warmth exchange at a limit (surface) inside a liquid, the Nusselt number is the proportion of convective to conductive warmth exchange crosswise over (typical to) the limit. In this unique situation, convection incorporates both shift in weather conditions and dissemination. The calculated Nusselt number for the heat transfer between the fluid and the rigid absorber tube is shown in Fig. 17. As shown heat transfer in the collector absorber increased as time goes on. Although the weak heat transfer cause decrease collector thermal performance, the lower pumping power is needed. Nusselt number for natural convection between absorber tube and glass versus time is shown in Fig. 18. A Nusselt number near one, to be specific convection and conduction of comparative greatness, is normal for "slug stream" or laminar stream. A bigger Nusselt number compares to increasingly dynamic convection, with tempestuous stream commonly in the 100 1000 territory.

As the liquid water flows along the tube, the collector liquid obtain the heat and its temperature rises. The simulations considered the heat transfer with buoyancy effects at the space between absorber tube and glass. Heat flux for natural convection between absorber tube and glass versus time is shown in Fig. 19. As shown the calculated heat flux is a significant heat transfer of the system. Since the heat loss from the supports is only a small part of heat loss from the collector, it is not considered.

Radiative Heat flux between absorber tube and glass and glass and sky versus time is shown in Fig. 20. Even though the collector panel is heated by a relatively weaker solar irradiance and has a lower solar collector fluid inlet temperature 30^oC, the fluid temperature at the end of the top tube rises above 50^oC. The heat loss is adjusted in such a way that the collector heat balance calculated with the first thermodynamics law is equal to the measured collector temperature difference. The heat flux into the absorber tube walls from the glass is significant and is not negligible.

In addition to the fact that the model includes heat transfer and buoyancy effects, the wind flow rate can affect on the energy transfer around the glass. Reynodls number of outside of the glass versus time is shown in Fig. 21. in spite of the case of inner tube plotted in Fig. 16 where the regime was laminar, here the regime is mostly turbulent.

Through the investigation the collector tilt angle are not considered. Forced convection Heat flux between glass and environment versus time is shown in Fig. 21. The collector is assumed to operate at a constant ambient temperature and to be heated with a weak solar irradiance. Such heat transfer is calculated by ignoring the buoyancy and longitudinal heat conduction . A comprehension of convection limit layers is important to understanding convective warmth exchange between a surface and a liquid streaming past it. A warm limit layer creates if the liquid free stream temperature and the surface temperatures contrast. A temperature profile exists because of the vitality trade coming about because of this temperature contrast. The heat loss from the absorber tube is assumed to be transferred only by means of forced convection which can be determined by a convective heat loss coefficient and the ambient air temperature. Forced convection Heat flux between glass and environment versus time is shown in Fig. 22. As shown the main heat loss of the system is occurred through the forced convection between thin glass and environment.

2.7 Exergy calculations

In this study, some lens is used to enhance the performance of a solar collector. The integrated solar collector is thermodynamically analyzed to trace the influence of changes in the solar collector design and operation on the promising performance. Therefore, the energy and exergy efficiencies are evaluated for the parabolic solar collector.

The temperature where the heat delivered and the pumping power affect the useful exergy production.

$$E_u = Q_u - m \cdot c_p \cdot T_o \cdot \ln\left[\frac{T_{out}}{T_{in}}\right] - \frac{m \cdot \mathrm{T}_o \cdot \Delta P}{\rho \cdot T_{fm}} \tag{8}$$

The exergy production rate which is available in environment versus time is shown in Fig. 23. It was found from Fig. 23 that the use of lens is the best technique according to the thermal, the exergy and the overall efficiency criteria. The exergy flow of the solar irradiation can not exceed the 93 percent of the solar irradiation:

$$E_{solar} = Q_{sun} \cdot \left[1 - \frac{4}{3} \cdot \frac{T_{amb}}{T_{sun}} + \frac{1}{3} \cdot \left(\frac{T_{amb}}{T_{sun}}\right)^4\right] \tag{9}$$

where T_{sun} is considered as 5770 K. Since the exergy efficiency is defined as

$$\eta_{ex} = \frac{E_u}{E_{solar}} \tag{10}$$

where plotted in Fig. 24. As the exergy efficiency is the net heat production as the maximum equivalent work that a Carnot thermal engine is able to produce. As shown when time increase the exergy efficiency of the system and the maximum exergy efficiency of the system was about 52 percent. The figures show that the most of the exergy is destroyed within the begining time solar field which represents about 90 percent of the total exergy destruction.

3 Conclusion

In the present study, a direct-absorption parabolic trough solar collector utilizing the lens has been proposed and investigated. In the proposed direct-absorption parabolic trough solar collector, we installed 23 lenses to centralize radiation at the top of the receiver tube so that the optical efficiency of the concentrated sun rays can be increased. Key factors influencing the collector performance have also been investigated. The following conclusions have been drawn.

- Cost implications of including the lenses in the system is 20 USD where compared to the price of the conventional systems is less than 10 percent. While adding the lenses increase the efficiency of the system more than 14 percent .
- The results show that using the solar concentrator increase the efficiency of Parabolic trough collector. Therefore, to achieve the same level of η_{th}, the lens supported solar thermal collector requires less solar radiation, which is beneficial for stable operation.
- The lens supported Parabolic trough solar thermal collector were found to be more desirable when $\dot{m} \leq 0.01$ kg/s, while the common Parabolic trough solar thermal collector works better for the higher flow rate (e.g., $\dot{m} > 0.01$ kg/s). This is because when $\dot{m} > 0.01$ kg/s, the temperature differences (ΔT) for all the cases are low, resulting in much less heat loss, especially for the common Parabolic trough solar thermal collector.
- We used RSME, MBE, CRM statistical criteria to calculate the errors and accuracy of the estimation of radiation. It was observed that the Angstrom method leads to a better correlations compared to the maximum probability.
- When the lenses were used, the fluid outlet temperature increased to a large extent, resulting in an increase in efficiency. For instance, at 13:30, lens efficiency increased from 43 percent to 57 percent.
- When time increase the exergy efficiency of the system and the maximum exergy efficiency of the system was about 52 percent.The use of lens enhance the exergy efficiency of the system.

The results obtained in this work will facilitate the use of lens in a parabolic trough solar collector with more stability and provide a guide for choosing suitable type of parabolic trough solar collectors for specific working conditions.

sortcompress

References

[1] İ. H. Yılmaz, A. Mwesigye, Modeling, simulation and performance analysis of parabolic trough solar collectors: A comprehensive review, Appl Energy 225 (2018) 135–174.

[2] S. A. Kalogirou, Solar energy engineering: processes and systems, Academic Press, 2013.

[3] M. Fan, H. Liang, S. You, H. Zhang, W. Zheng, J. Xia, Heat transfer analysis of a new volumetric based receiver for parabolic trough solar collector, Energy 142 (2018) 920–931.

[4] J. P. Freedman, H. Wang, R. S. Prasher, Analysis of nanofluid-based parabolic trough collectors for solar thermal applications, J Sol Energ Eng 140 (5) (2018) 051008.

[5] V. Khullar, H. Tyagi, P. E. Phelan, T. P. Otanicar, H. Singh, R. A. Taylor, Solar energy harvesting using nanofluids-based concentrating solar collector, J Nanotechnol Eng Med 3 (3) (2012) 031003.

[6] H. Tyagi, P. Phelan, R. Prasher, Predicted efficiency of a low-temperature nanofluid-based direct absorption solar collector, J Sol Energ Eng 131 (4) (2009) 041004.

[7] T. Otanicar, P. E. Phelan, R. S. Prasher, G. Rosengarten, R. A. Taylor, Nanofluid-based direct absorption solar collector, J Renew Sustain Ener 2 (3) (2010) 033102.

[8] E. Sani, L. Mercatelli, S. Barison, C. Pagura, F. Agresti, L. Colla, P. Sansoni, Potential of carbon nanohorn-based suspensions for solar thermal collectors, Sol Energ Mat Sol C 95 (11) (2011) 2994–3000.

[9] B. J. Lee, K. Park, T. Walsh, L. Xu, Radiative heat transfer analysis in plasmonic nanofluids for direct solar thermal absorption, J Sol Energ Eng 134 (2) (2012) 021009.

[10] A. Veeraragavan, A. Lenert, B. Yilbas, S. Al-Dini, E. N. Wang, Analytical model for the design of volumetric solar flow receivers, Int J Heat Mass Tran 55 (4) (2012) 556–564.

[11] H. K. Gupta, G. D. Agrawal, J. Mathur, Investigations for effect of Al_2O_3-H_2O nanofluid flow rate on the efficiency of direct absorption solar collector, Case Studies in Thermal Eng 5 (2015) 70–78.

[12] V. Cregan, T. Myers, Modelling the efficiency of a nanofluid direct absorption solar collector, Int J Heat Mass Tran 90 (2015) 505–514.

[13] T. B. Gorji, A. A. Ranjbar, Geometry optimization of a nanofluid-based direct absorption solar collector using response surface methodology, Sol Energy 122 (2015) 314–325.

[14] J. Jeon, S. Park, B. J. Lee, Analysis on the performance of a flat-plate volumetric solar collector using blended plasmonic nanofluids, Sol Energy 132 (2016) 247–256.

[15] C. Qin, K. Kang, I. Lee, B. J. Lee, Optimization of a direct absorption solar collector with blended plasmonic nanofluids, Sol Energy 150 (2017) 512–520.

[16] K. H. Won, B. J. Lee, Effect of light scattering on the performance of a direct absorption solar collector, Front Energy 12 (1) (2018) 169–177.

[17] C. Qin, K. Kang, I. Lee, B. J. Lee, Optimization of the spectral absorption coefficient of a plasmonic nanofluid for a direct absorption solar collector, Sol Energy 169 (2018) 231–236.

[18] A. R. Mallah, S. Kazi, M. N. M. Zubir, A. Badarudin, Blended morphologies of plasmonic nanofluids for direct absorption applications, Appl Energy 229 (2018) 505–521.

[19] J. Jeon, S. Park, B. J. Lee, Optical property of blended plasmonic nanofluid based on gold nanorods, Opt Express 22 (104) (2014) A1101–A1111.

[20] M. Chen, Y. He, J. Zhu, B. Jiang, Y. Huang, An experimental investigation on sunlight absorption characteristics of silver nanofluids, Sol Energy 115 (2015) 85–94.

[21] M. Chen, Y. He, J. Zhu, D. R. Kim, Enhancement of photo-thermal conversion using gold nanofluids with different particle sizes, Energ Convers Manage 112 (2016) 21–30.

[22] M. Du, G. H. Tang, Plasmonic nanofluids based on gold nanorods/nanoellipsoids/nanosheets for solar energy harvesting, Sol Energy 137 (2016) 393–400.

[23] V. Bhalla, H. Tyagi, Parameters influencing the performance of nanoparticles-laden fluid-based solar thermal collectors: A review on optical properties, Renew Sustain Energ Rev 84 (2018) 12–42.

[24] Z. Wang, Z. M. Zhang, X. Quan, P. Cheng, A numerical study on effects of surrounding medium, material, and geometry of nanoparticles on solar absorption efficiencies, Int J Heat Mass Tran 116 (2018) 825–832.

[25] A. Menbari, A. A. Alemrajabi, A. Rezaei, Heat transfer analysis and the effect of CuO/water nanofluid on direct absorption concentrating solar collector, Appl Therm Eng 104 (2016) 176–183.

[26] G. J. O'Keeffe, S. L. Mitchell, T. G. Myers, V. Cregan, Modelling the efficiency of a low-profile nanofluid-based direct absorption parabolic trough solar collector, Int J Heat Mass Tran 126 (2018) 613–624.

[27] G. J. O'Keeffe, S. L. Mitchell, T. G. Myers, V. Cregan, Modelling the efficiency of a nanofluid-based direct absorption parabolic trough solar collector, Sol Energy 159 (2018) 44–54.

[28] C. F. Bohren, D. R. Huffman, Absorption and Scattering of Light by Small Particles, Wiley, 1983.

[29] A. De Risi, M. Milanese, D. Laforgia, Modelling and optimization of transparent parabolic trough collector based on gas-phase nanofluids, Renew Energy 58 (2013) 134–139.

[30] F. P. Incropera, D. P. Dewitt, T. L. Bergman, A. S. Lavine, Principles of heat and mass transfer, John Wiley & Sons, 2013.

[31] T. B. Gorji, A. A. Ranjbar, A numerical and experimental investigation on the performance of a low-flux direct absorption solar collector (DASC) using graphite, magnetite and silver nanofluids, Sol Energy 135 (2016) 493–505.

[32] Z. D. Cheng, Y. L. He, F. Q. Cui, B. C. Du, Z. J. Zheng, Y. Xu, Comparative and sensitive analysis for parabolic trough solar collectors with a detailed Monte Carlo ray-tracing optical model, Appl Energy 115 (2014) 559–572.

[33] Q. Li, C. Zheng, S. Mesgari, Y. L. Hewkuruppu, N. Hjerrild, F. Crisostomo, G. Rosengarten, J. A. Scott, R. A. Taylor, Experimental and numerical investigation of volumetric versus surface solar absorbers for a concentrated solar thermal collector, Sol Energy 136 (2016) 349–364.

[34] D. Rativa, L. A. Gómez-Malagón, Solar radiation absorption of nanofluids containing metallic nanoellipsoids, Sol Energy 118 (2015) 419–425.

[35] Solutia, Therminol VP-1 Vapor Phase, Liquid Phase Heat Transfer Fluid 12°C to 400°C, http://twt.mpei.ac.ru/tthb/hedh/htf-vp1.pdf (2013).

[36] A. Lenert, E. N. Wang, Optimization of nanofluid volumetric receivers for solar thermal energy conversion, Sol Energy 86 (1) (2012) 253–265.

[37] S. Dugaria, M. Bortolato, D. Del Col, Modelling of a direct absorption solar receiver using carbon based nanouids under concentrated solar radiation, Renew Energy 128 (2018) 495–508.

[38] B. E. Launder, D. B. Spalding, The numerical computation of turbulent flows, in: Numerical Prediction of Flow, Heat Transfer, Turbulence and Combustion, Elsevier, 1983, pp. 96–116.

[39] T. L. Bergman, F. P. Incropera, D. P. DeWitt, A. S. Lavine, Fundamentals of heat and mass transfer, John Wiley & Sons, 2011.

[40] W. M. Kays, Turbulent prandtl number – where are we?, J Heat Transf 116 (2) (1994) 284–295.

[41] R. Forristall, Heat transfer analysis and modeling of a parabolic trough solar receiver implemented in engineering equation solverdoi:10.2172/15004820.

[42] G. Xu, W. Chen, S. Deng, X. Zhang, S. Zhao, Performance evaluation of a nanofluid-based direct absorption solar collector with parabolic trough concentrator, Nanomaterials 5 (4) (2015) 2131–2147.

[43] F. Wang, Q. Lai, H. Han, J. Tan, Parabolic trough receiver with corrugated tube for improving heat transfer and thermal deformation characteristics, Appl Energy 164 (2016) 411–424.

[44] W. C. Swinbank, Long-wave radiation from clear skies, Q J Roy Meteor Soc 89 (381) (1963) 339–348.

[45] J. A. Duffie, W. A. Beckman, Solar Engineering of Thermal Processes, John Wiley & Sons, 2013.

[46] V. E. Dudley, G. J. Kolb, A. R. Mahoney, T. R. Mancini, C. W. Matthews, M. Sloan, D. Kearney, Test results: SEGS LS-2 solar collector (1994).

Table 1: Characteristics of the collector in the East-West direction exposed to the south

property	value	unit
Length of the collector	1.8	m
Width of the collector	1	m
Depth of the collector	0.8	m
Tilt angle of the collector	45	degree
Concentration coefficient of the collector	3	-
Thickness of the absorber tube	5	mm
Diameter of the absorber tube	70	mm
Outer diameter of the glass	100	mm
Thickness of the glass	4	mm
Thermal conductivity of the metal tube	80	w/mk
Emmissivity coefficient of the absorber tube	0.13	-
Emmissivity coefficient of the glass	0.8	-
Thermal conductivity of the glass	1.13	w/mk

Table 2: Error of calculation methods

Day	RMSE angstrom	RMSE max possibility	MBE angstrom	MBE max possibility	CRM angstrom	CRM max possibility
8	0.0076	3.2447	0.0329	-0.6808	-0.0009	0.0182
9	2.9277	13.0292	-0.6467	-1.3643	0.017	0.0359
10	12.1857	6.5558	-1.3194	-0.9678	0.0352	0.0258
11	0.2111	2.1002	0.1737	-0.5478	-0.0047	0.0148
12	3.4632	14.1886	-0.7034	-1.4237	0.0185	0.0374
13	13.3313	19.2949	-1.38	-1.6602	0.0358	0.0431
14	0.2278	6.8343	-0.1804	-0.9881	0.0048	0.0261
15	2.3283	12.9938	-0.5767	-1.3624	0.0152	0.036

Table 3: Numerical and experimental calculation of the solar radiation

Date	n	N	angstrom	max possibility	measurements
8/7/2018	10.34611111	14.284	523.1923077	513	522.7316429
9/7/2018	10.34305556	14.26266667	522.5461538	512.5	531.6002143
10/7/2018	9.5975	14.25466667	505.8769231	510.8	524.3485
11/7/2018	10.05444444	14.24	520.5	510.4	518.0685714
12/7/2018	10.43638889	14.224	523.3846154	513.3	533.2319286
13/7/2018	10.29972222	14.204	519.9230769	516	539.2434286
14/7/2018	10.67638889	14.19066667	527.3076923	516	529.8333571
15/7/2018	10.45361111	14.172	522	511	530.0742143

Table 4: Measuring instruments specifications

Measuring instruments	Ranges	Accuracy	Error
Solarimeter	(0 5000) W/m^2	1 W/m^2	0.46
Thermocouples	(0100) ^oC	0.1 ^oC	0.195
Vane anemometer	(0.4 30) m/s	0.1 m/s	2.43
Calibrated container	(0 2000) ml	5 ml	0.25

Figure 1: Parabolic trough at a plant near Harper Lake, California. CrossRef

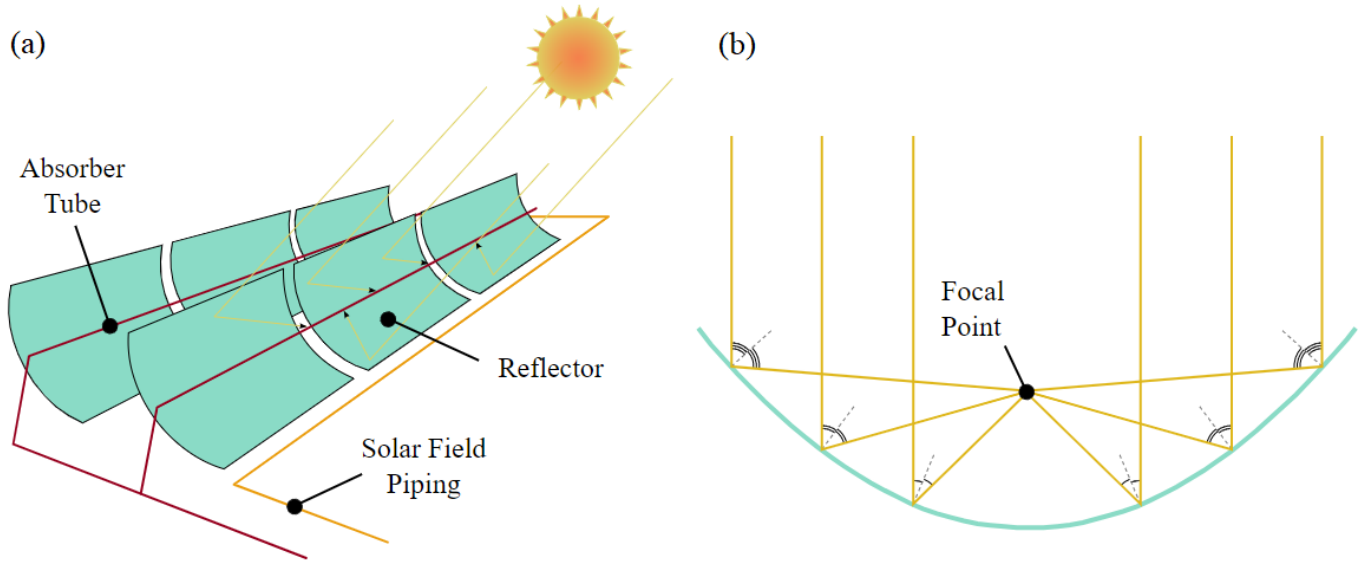

Figure 2: (a) A diagram of a parabolic trough solar farm , and (b) an end view of how a parabolic collector focuses sunlight onto its focal point.CrossRef

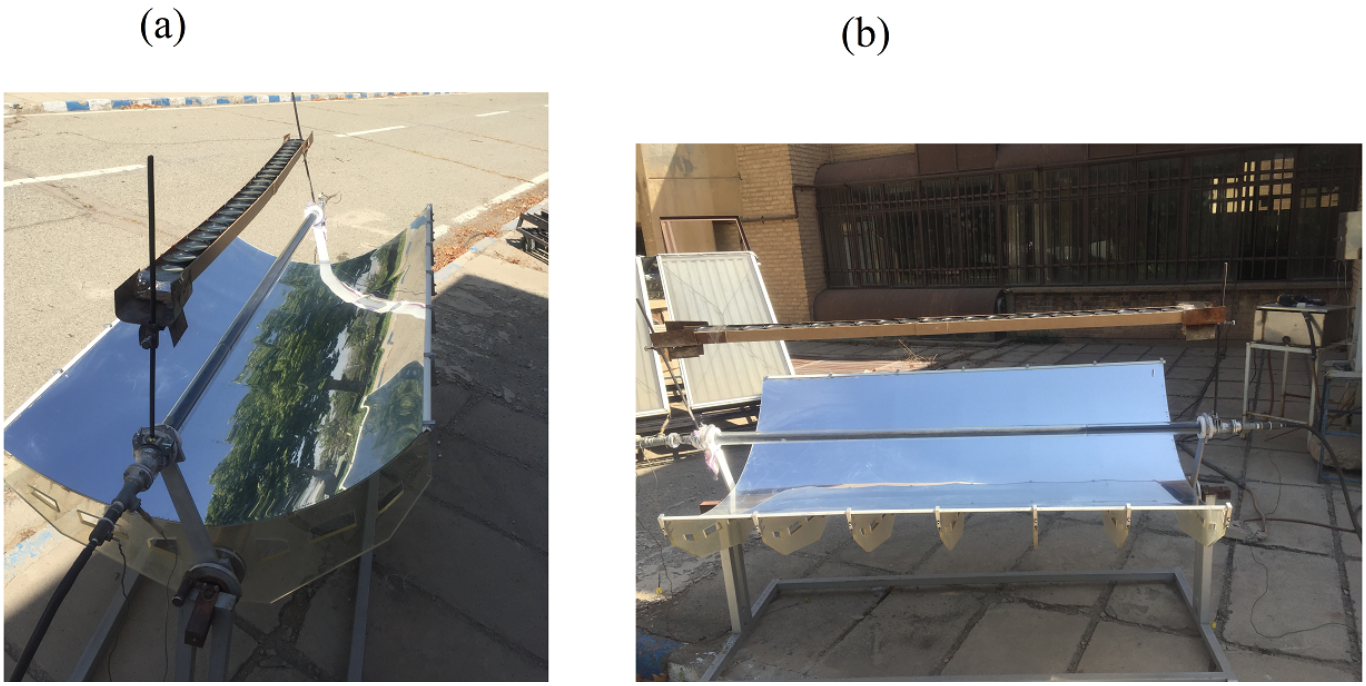

Figure 3: Experimental setup. (a) isometric view (b) front view

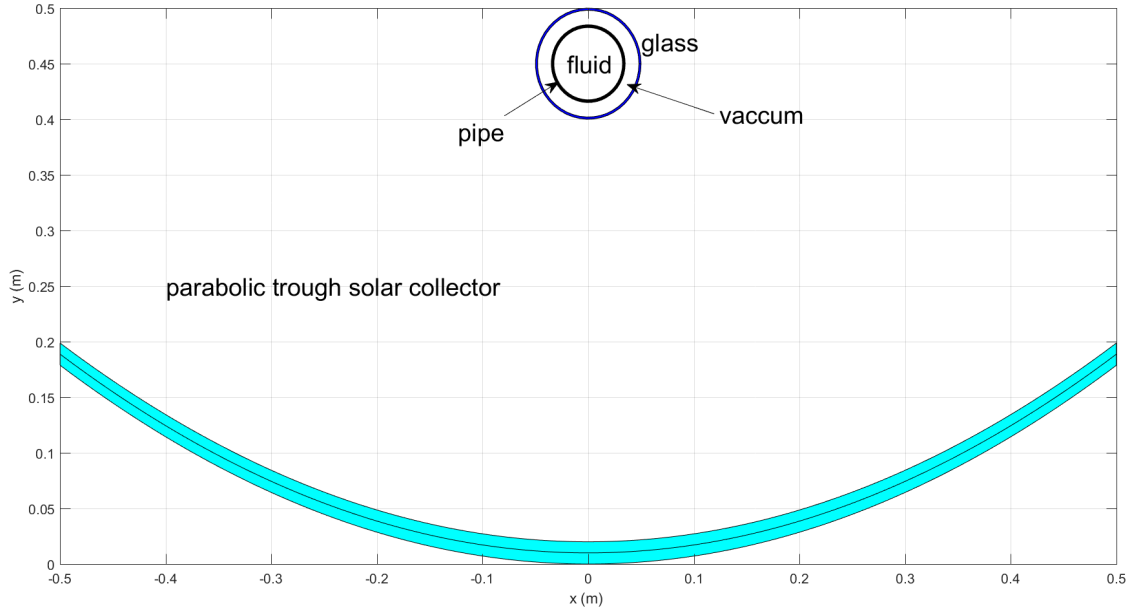

Figure 4: Cross section of device

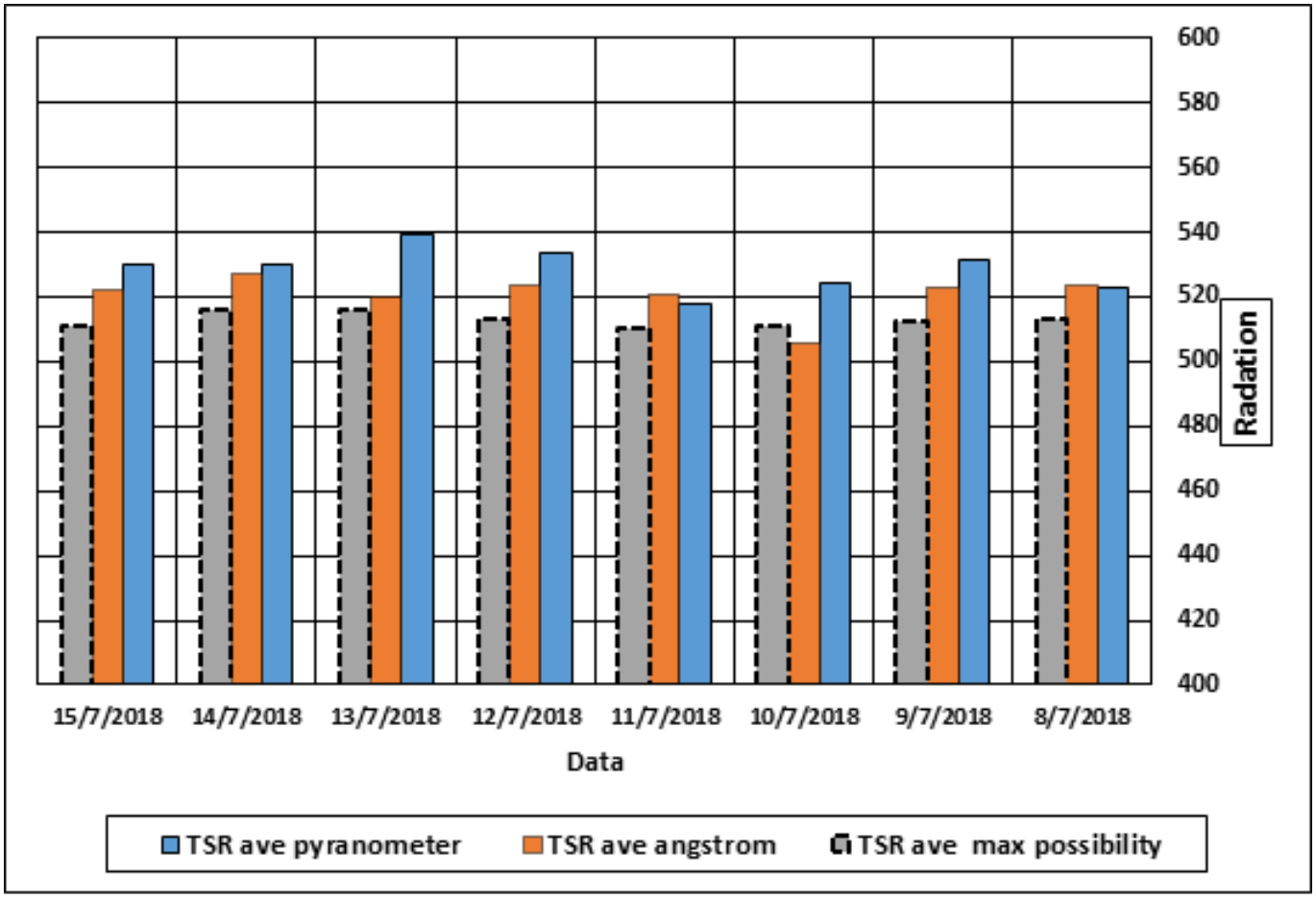

Figure 5: Numerical and experimental calculation of the solar radiation

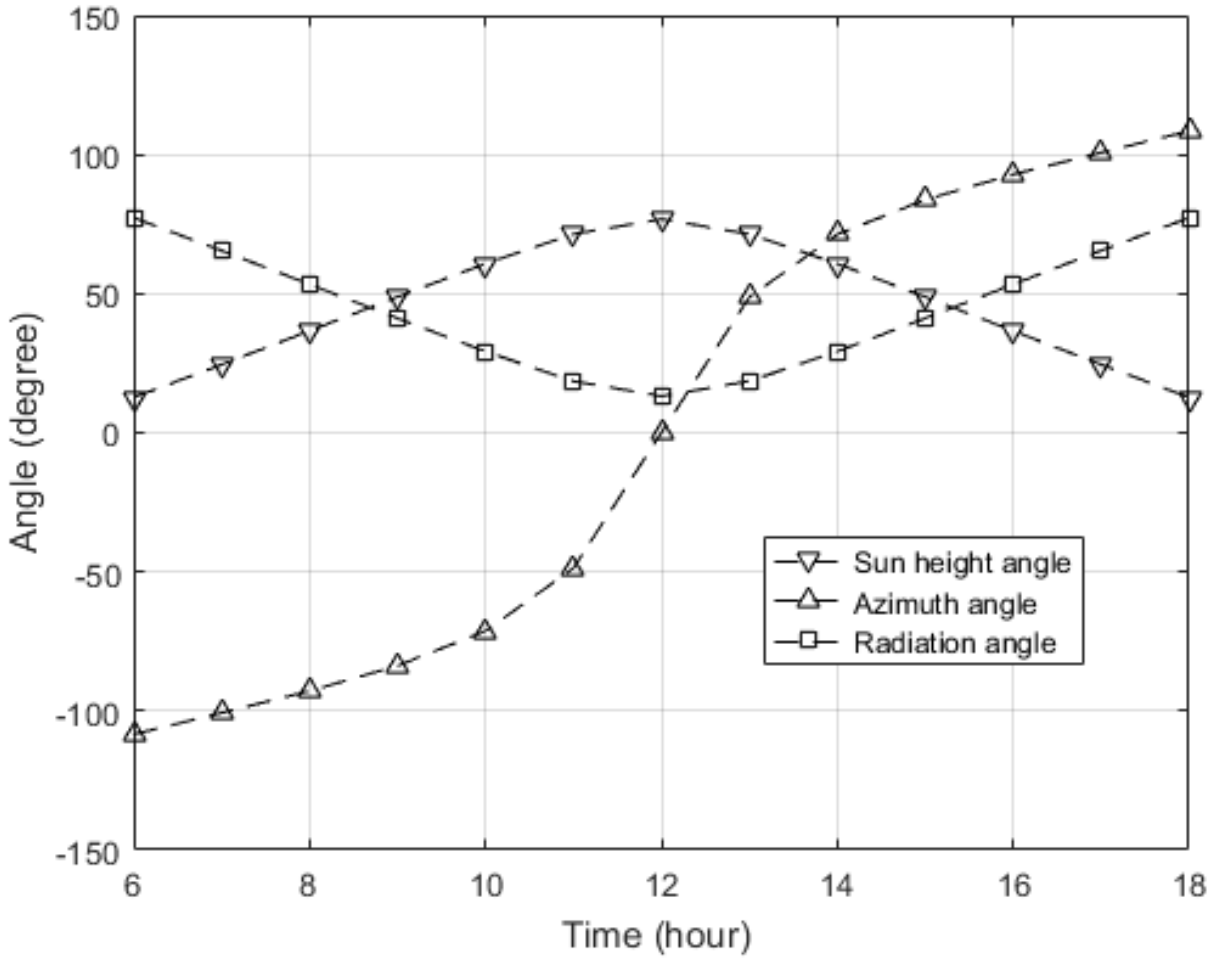

Figure 6: Sun angles vs time on 15/7/2018.

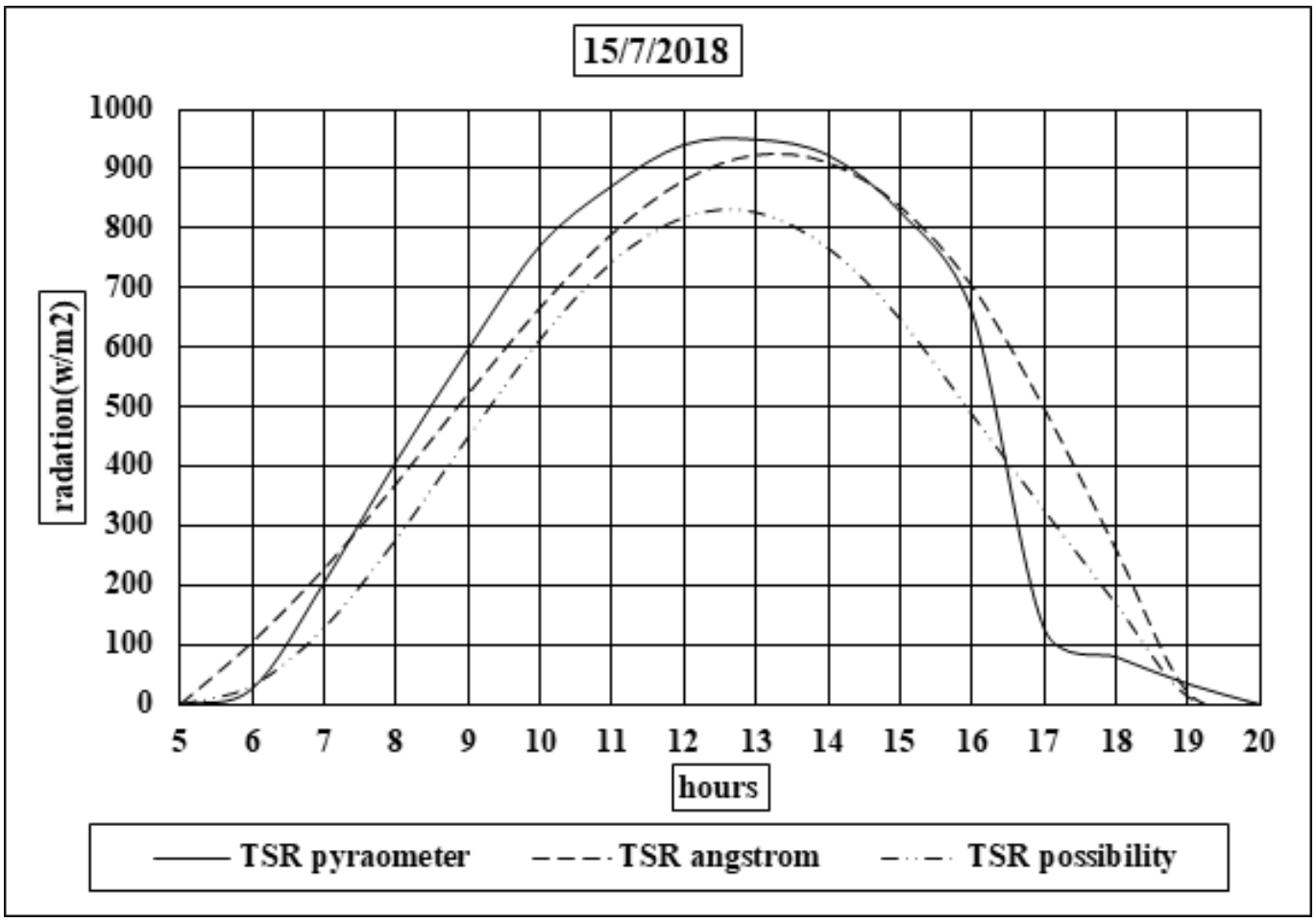

Figure 7: Radiation vs time on 15/7/2018.

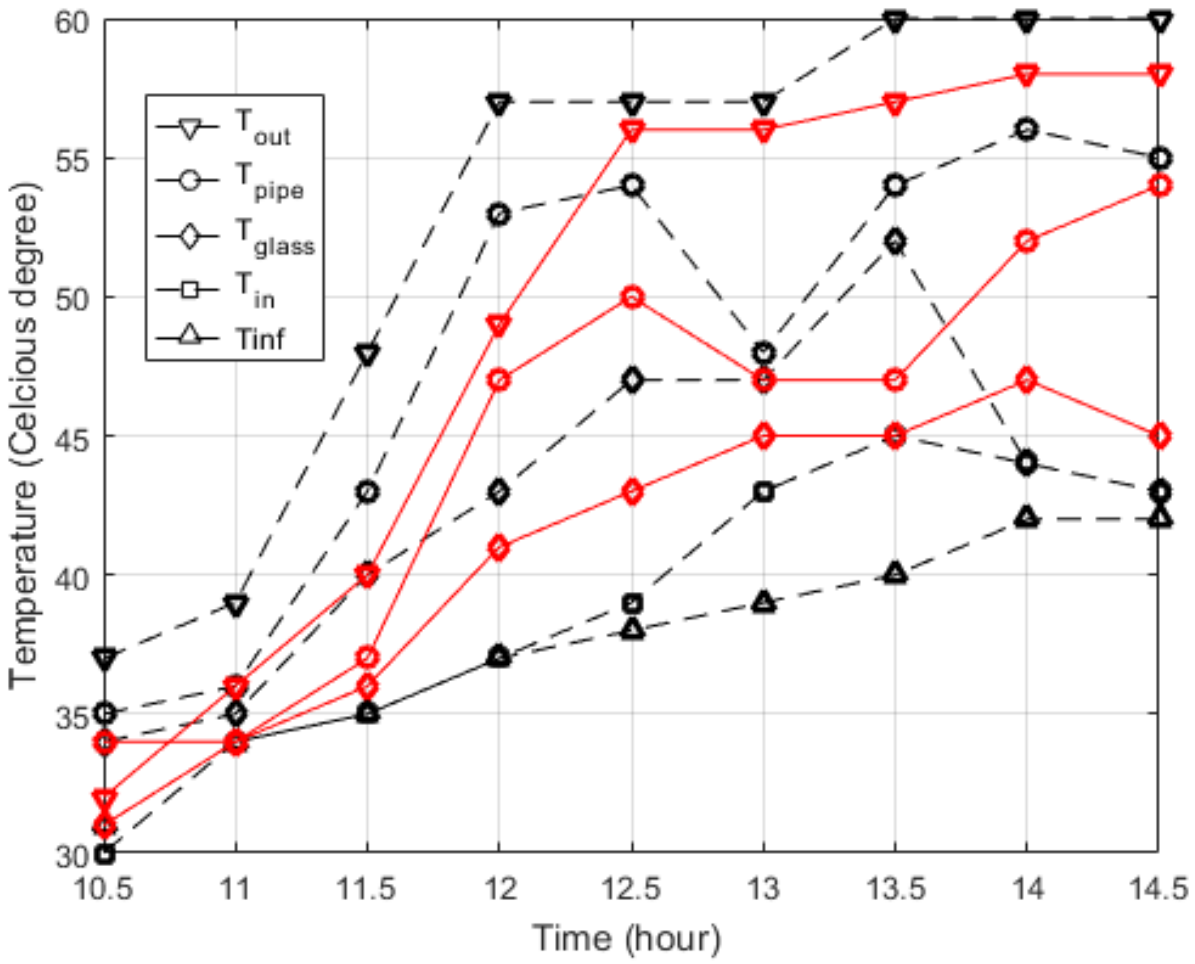

Figure 8: Temperatures in various position of the devices versus time

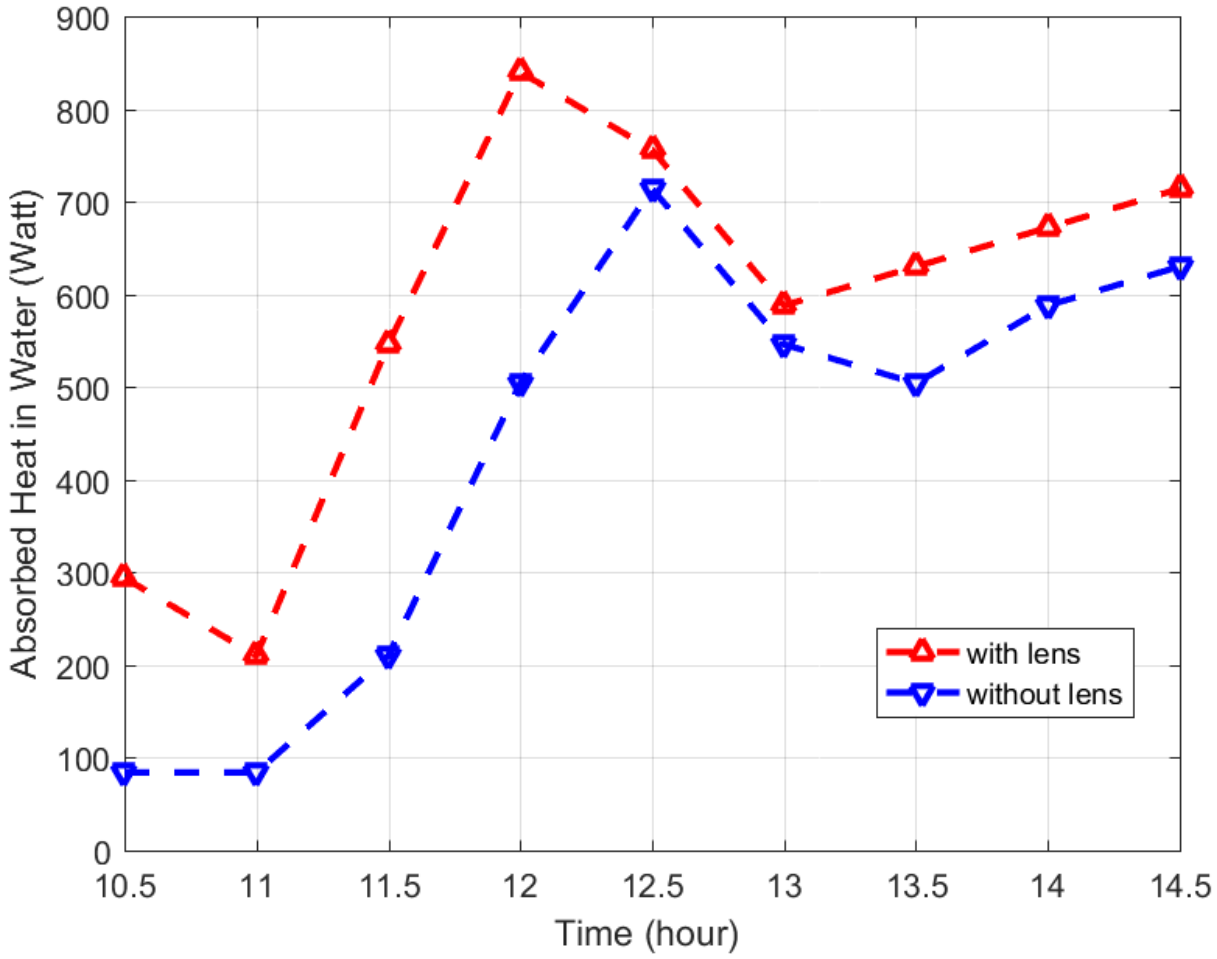

Figure 9: Absorbed Heat in Water vs time on 10/7/2018

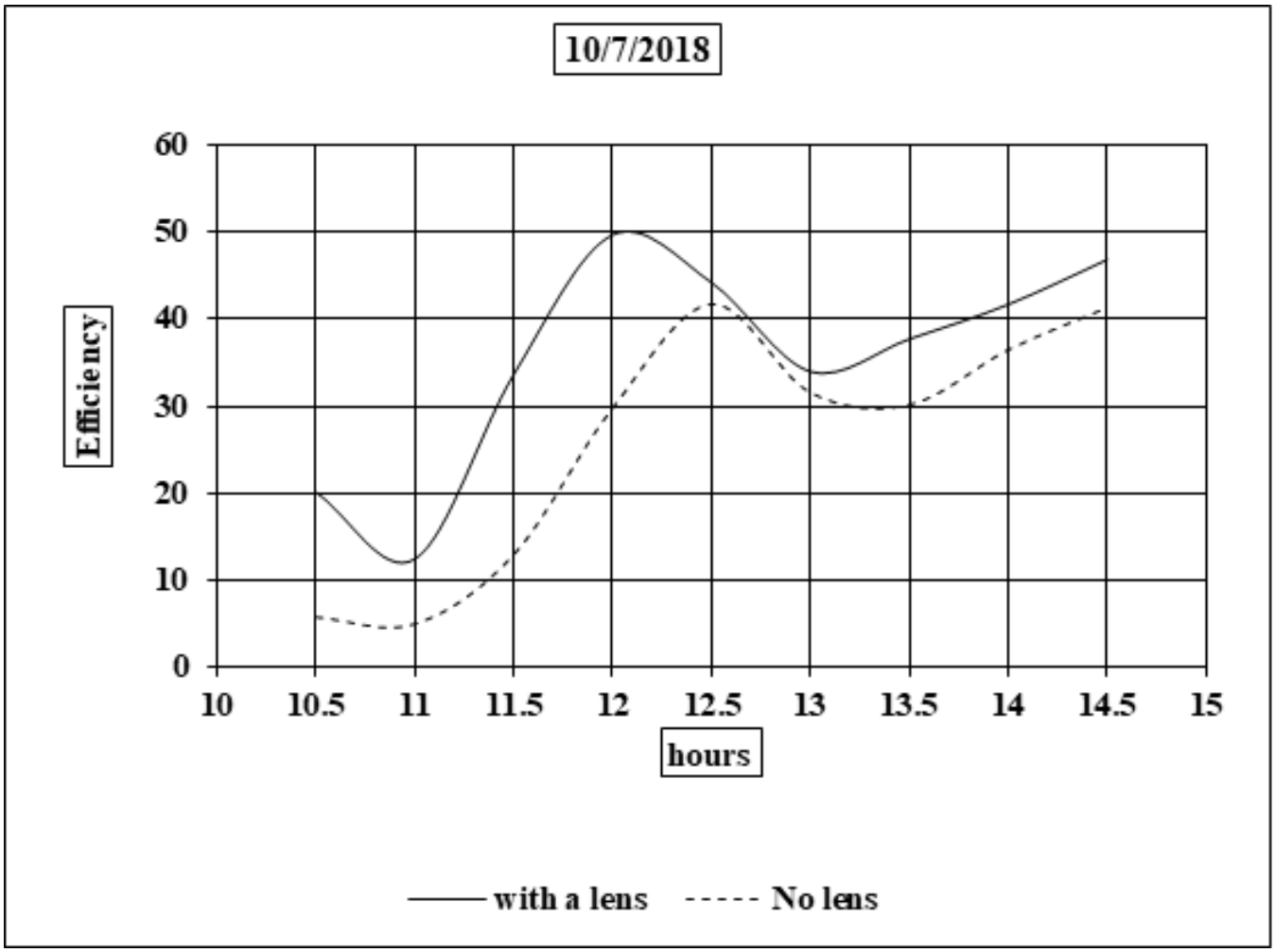

Figure 10: Efficiency of the system versus time on 10/7/2018. solid line are the case without lens and dashed line are the case with lens.

Figure 11: Velocity meter

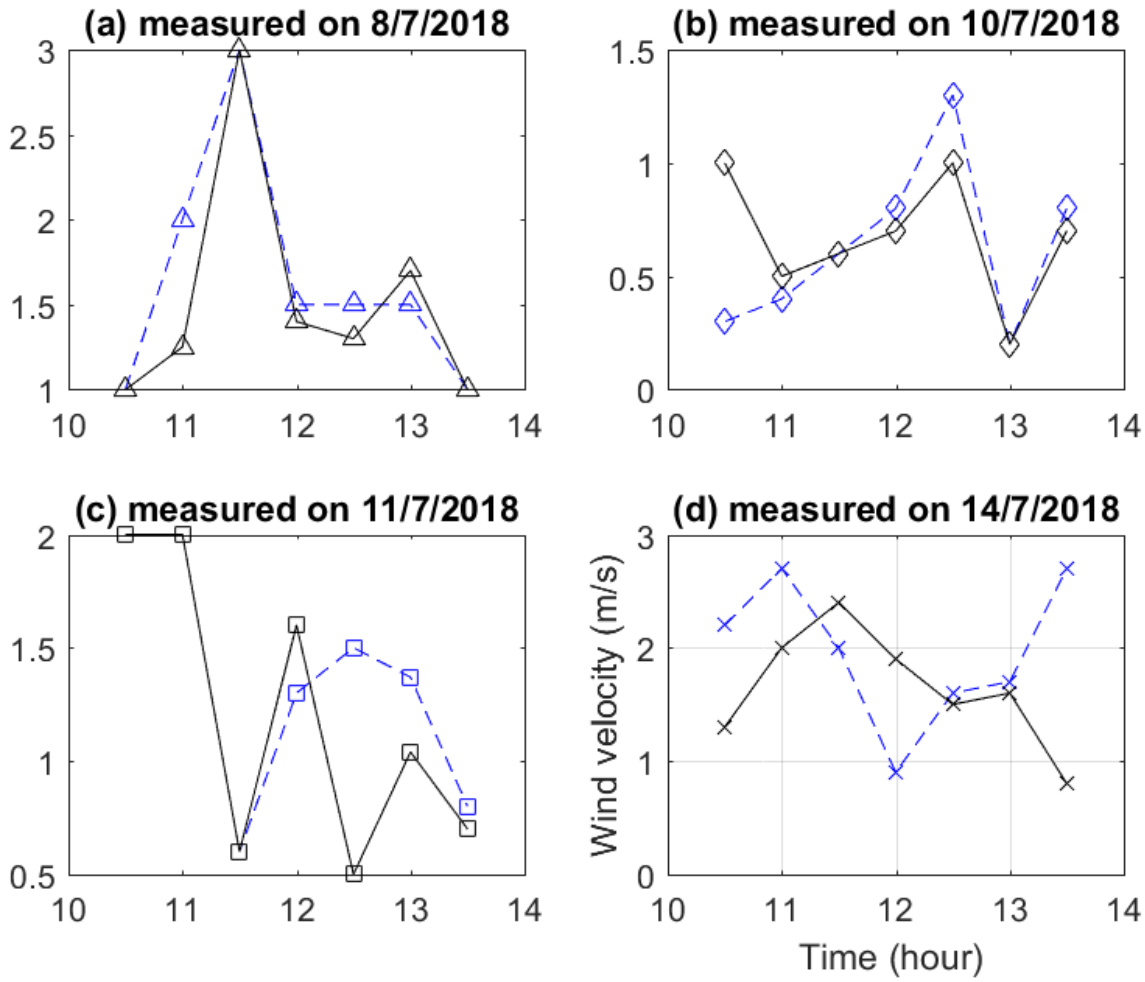

Figure 12: Wind velocity versus time. solid line are the case without lens and dashed line are the case with lens.

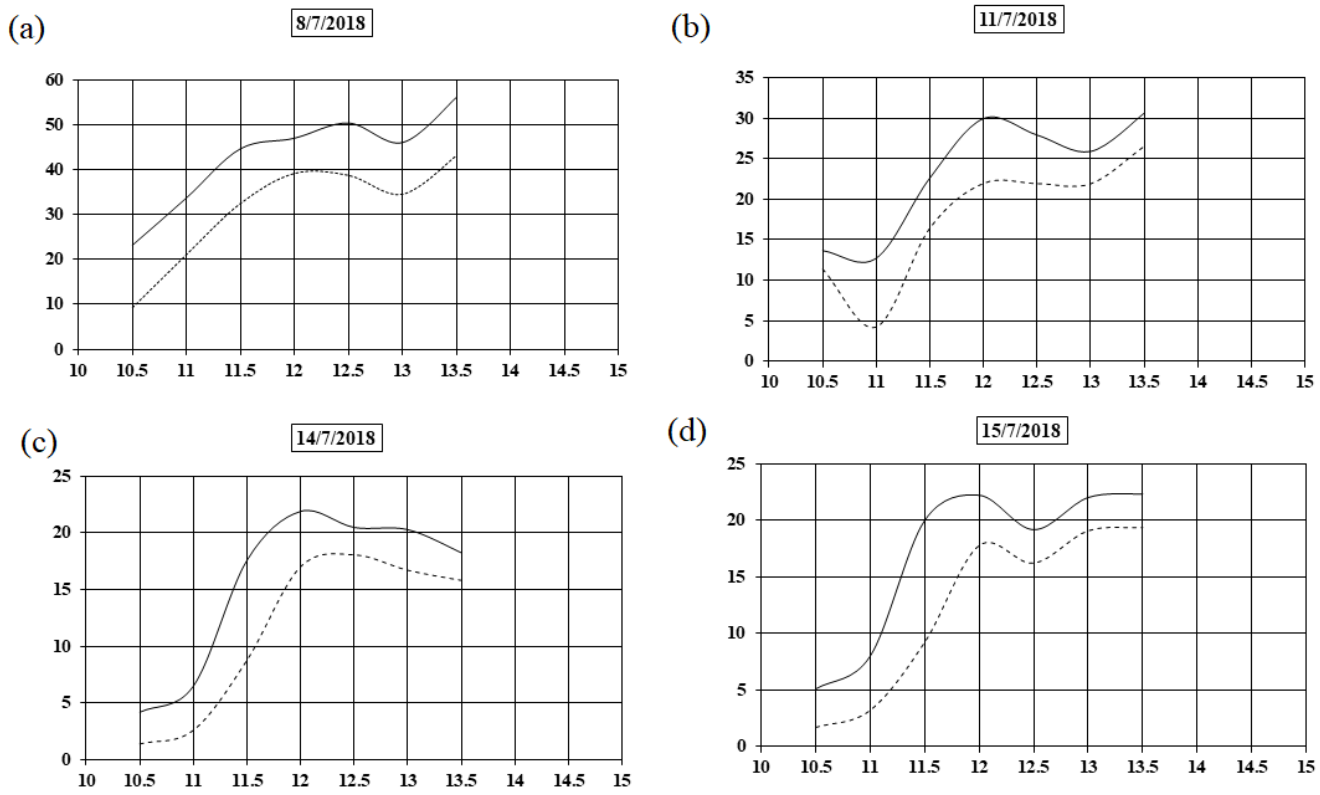

Figure 13: Efficiency percent versus time. solid line are the case without lens and dashed line are the case with lens.

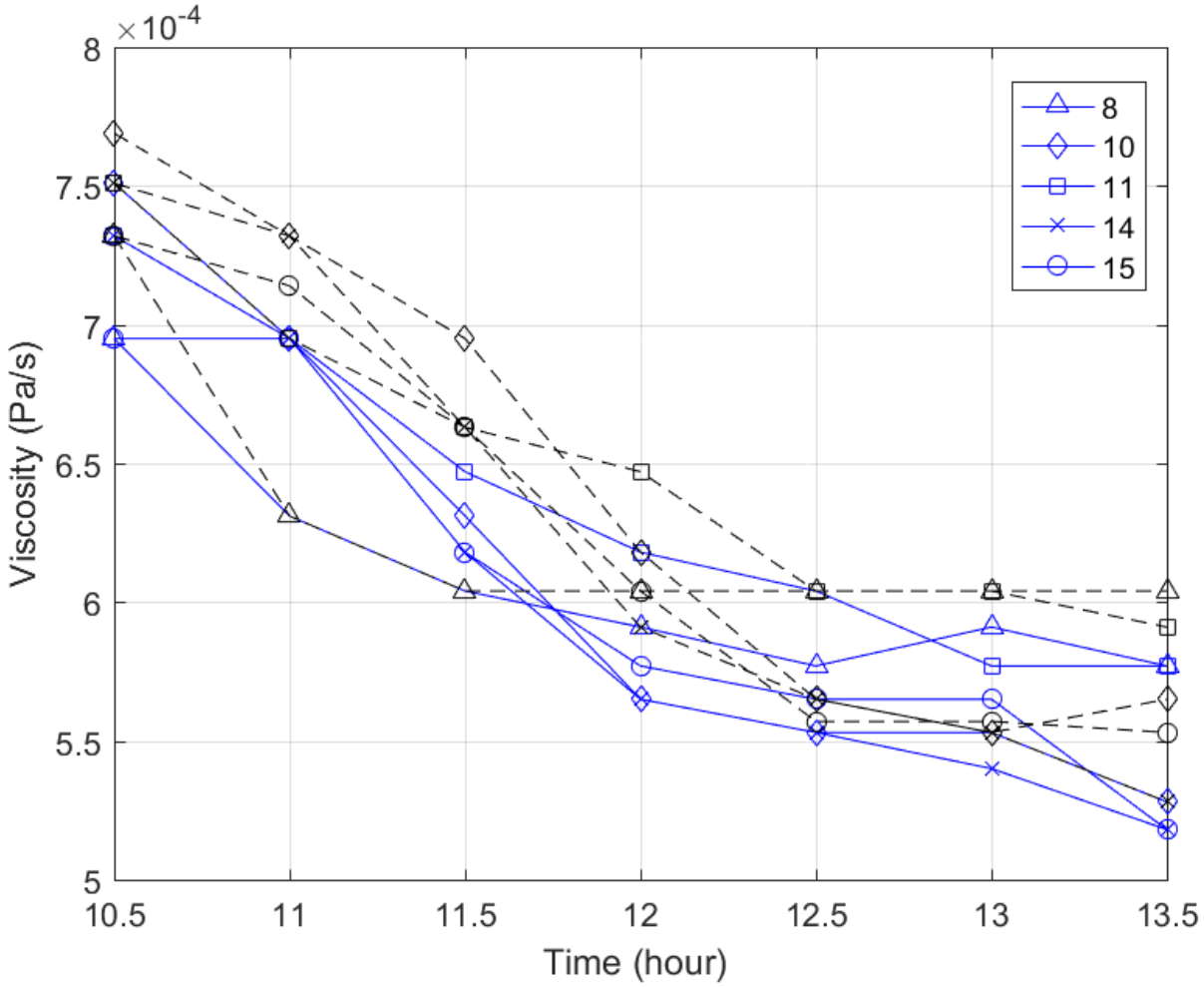

Figure 14: Visosity versus time. solid line are the case without lens and dashed line are the case with lens.

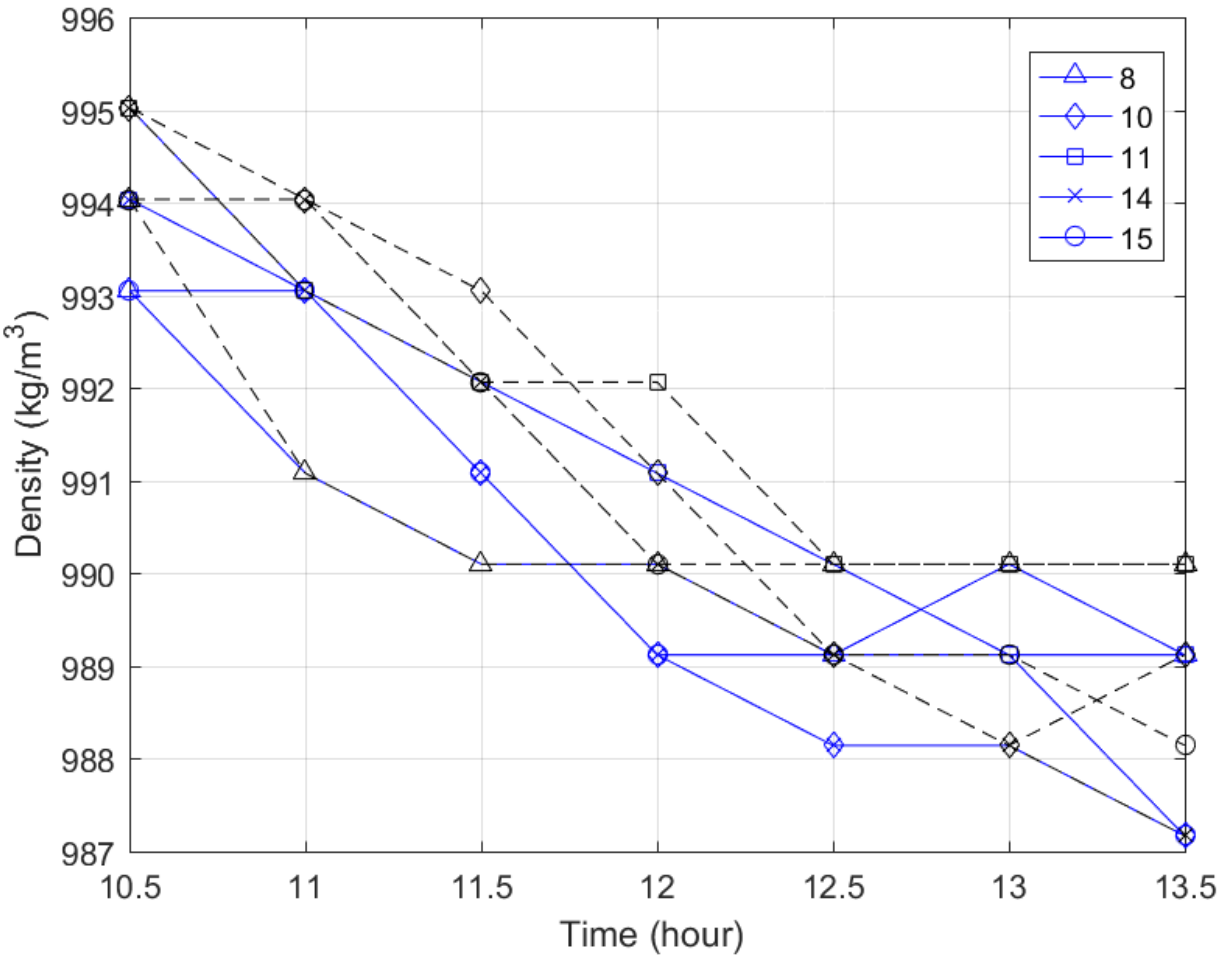

Figure 15: Density versus time. solid line are the case without lens and dashed line are the case with lens.

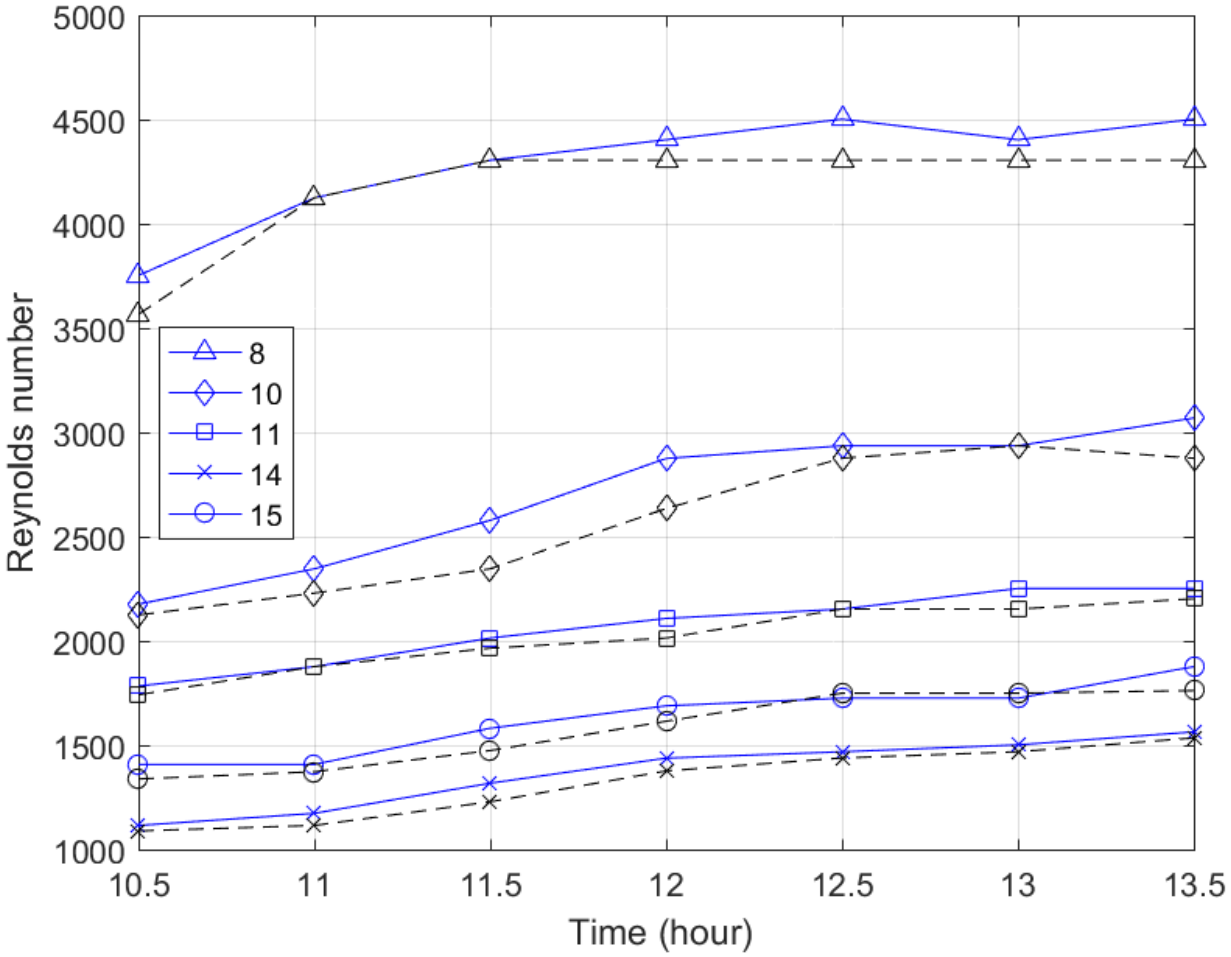

Figure 16: Reynolds number versus time. solid line are the case without lens and dashed line are the case with lens.

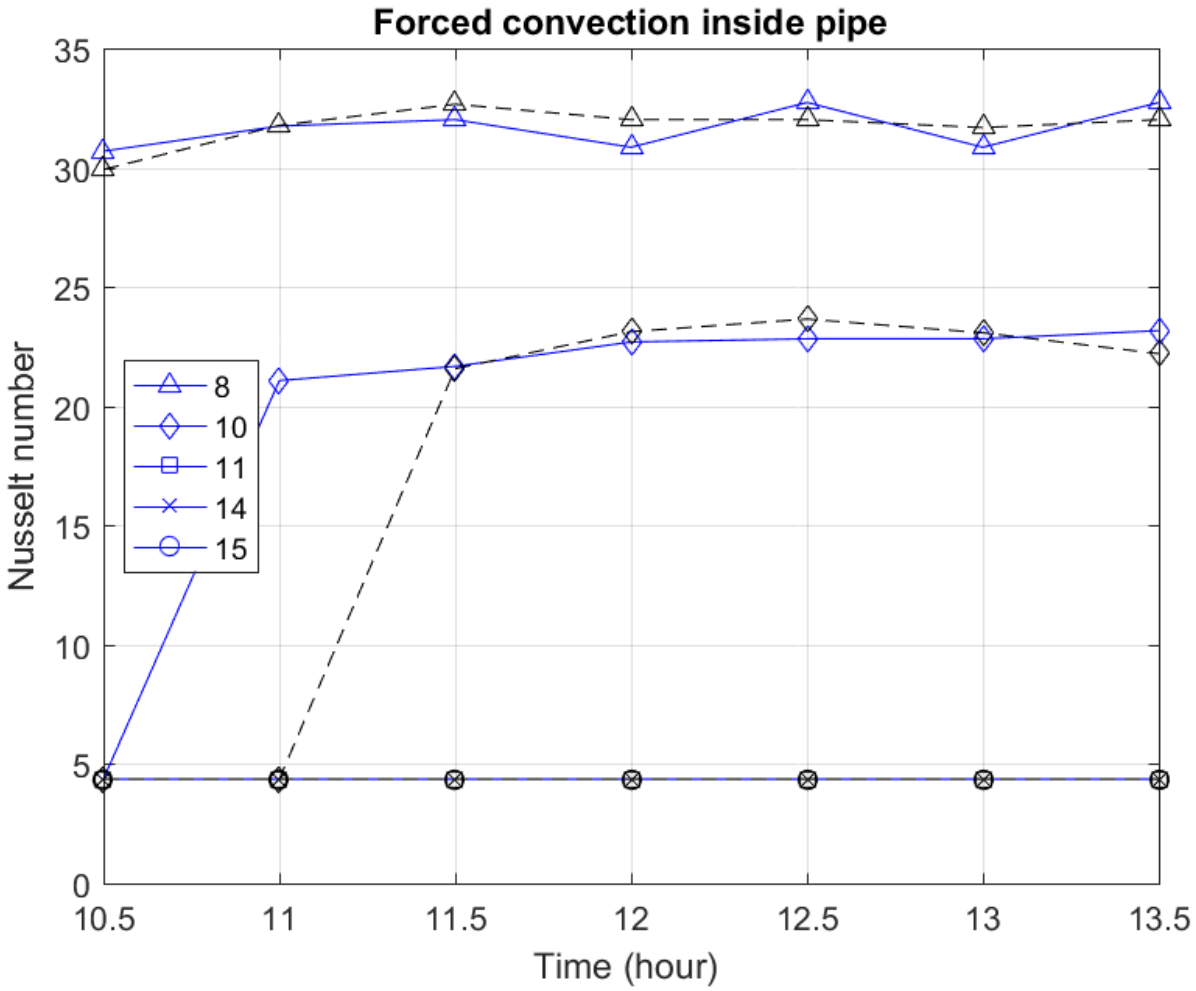

Figure 17: Nusselt number for forced convection inside tube versus time. solid line are the case without lens and dashed line are the case with lens.

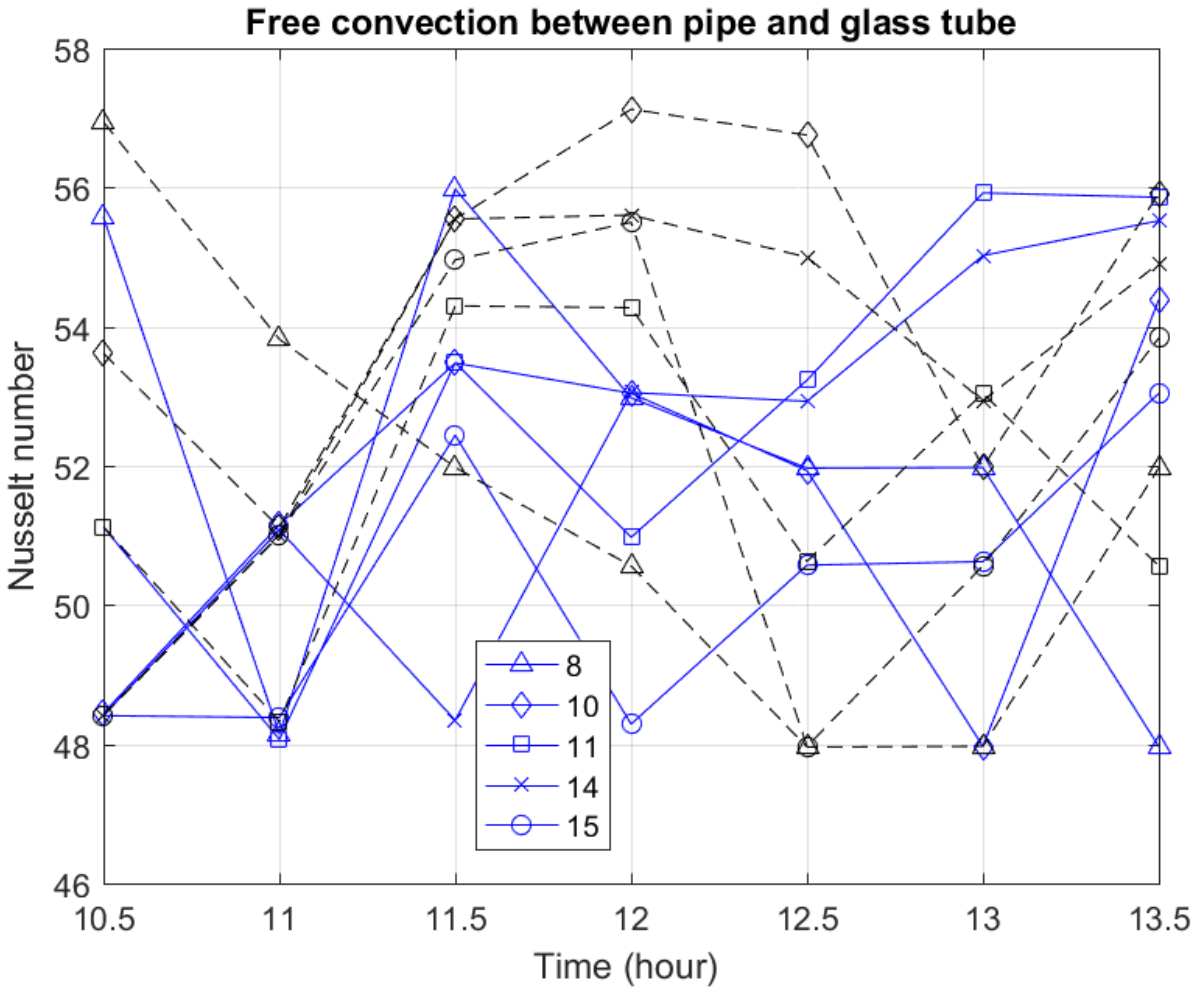

Figure 18: Nusselt number for natural convection between absorber tube and glass versus time. solid line are the case without lens and dashed line are the case with lens.

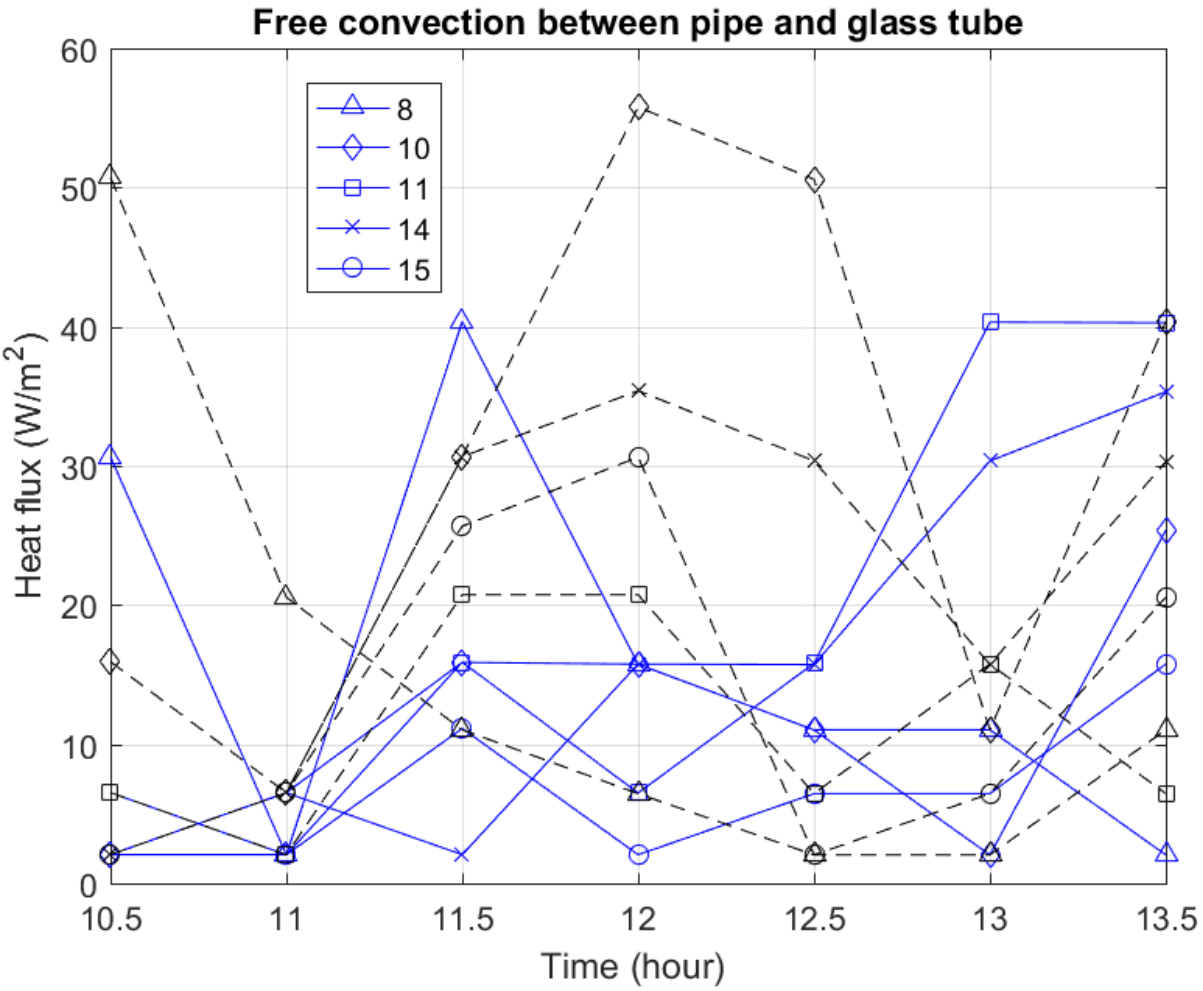

Figure 19: Heat flux for natural convection between absorber tube and glass versus time. solid line are the case without lens and dashed line are the case with lens.

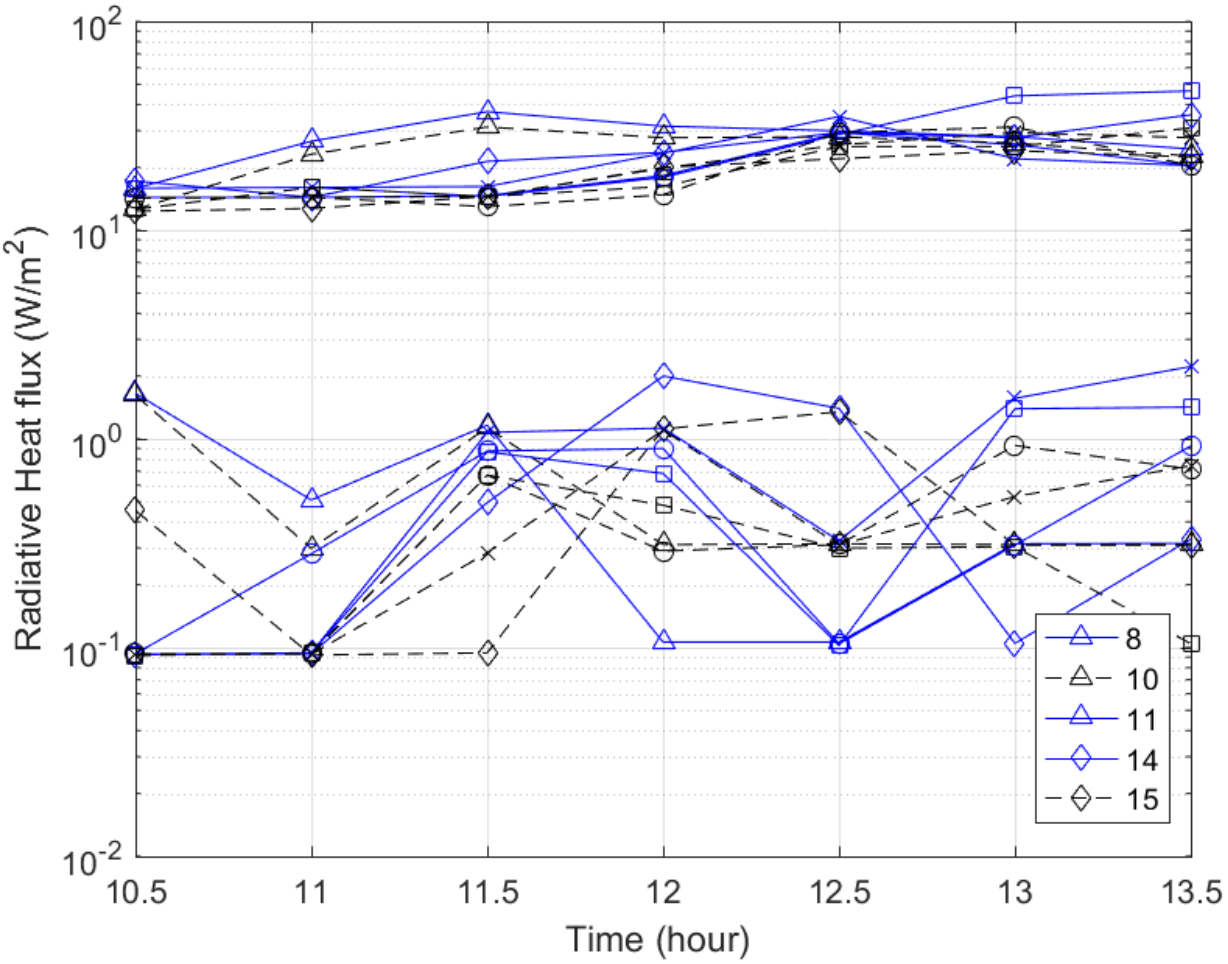

Figure 20: Radiative Heat flux between absorber tube and glass and glass and sky versus time. solid line are the case without lens and dashed line are the case with lens.

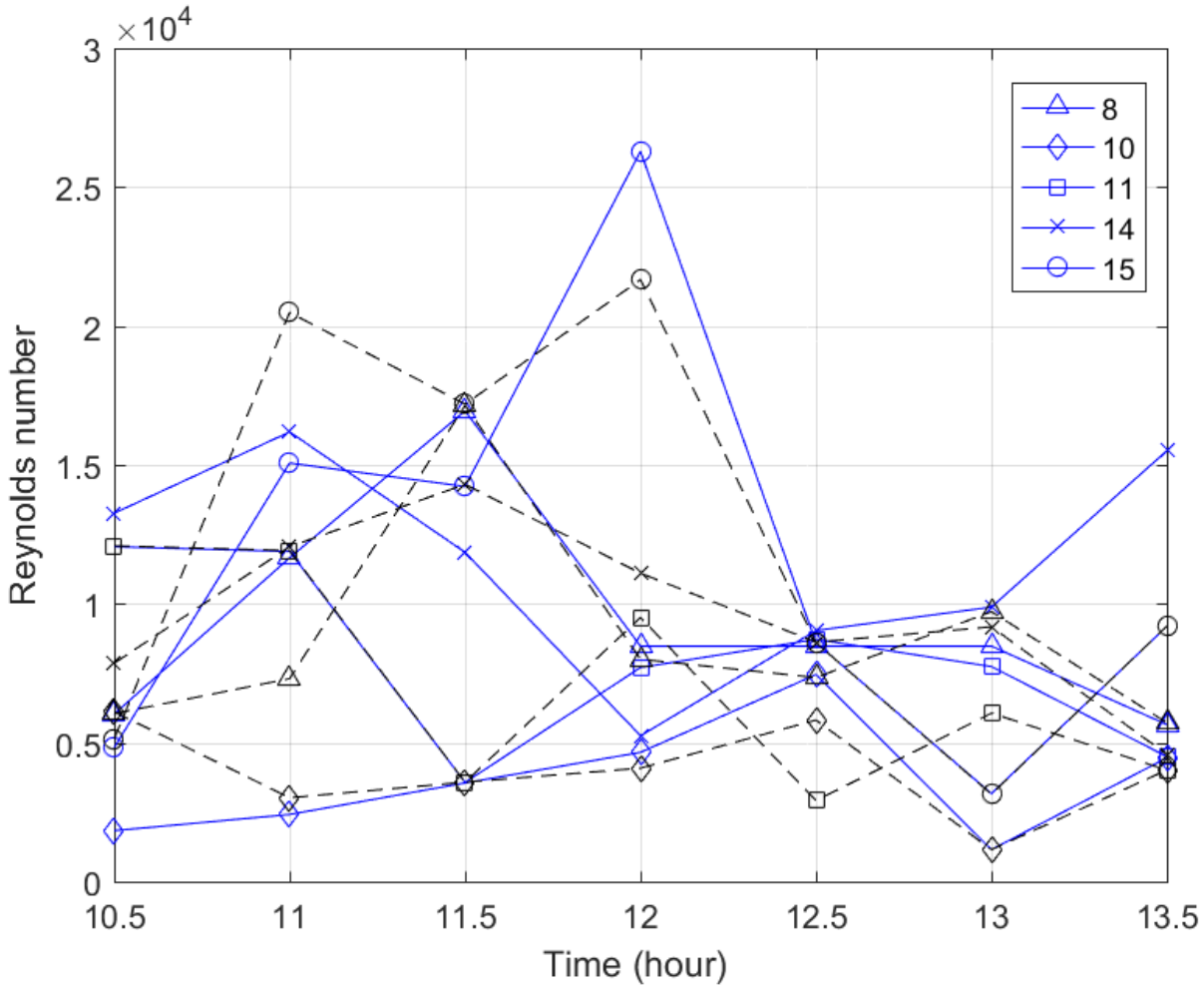

Figure 21: Reynodls number of outside of the glass versus time. solid line are the case without lens and dashed line are the case with lens.

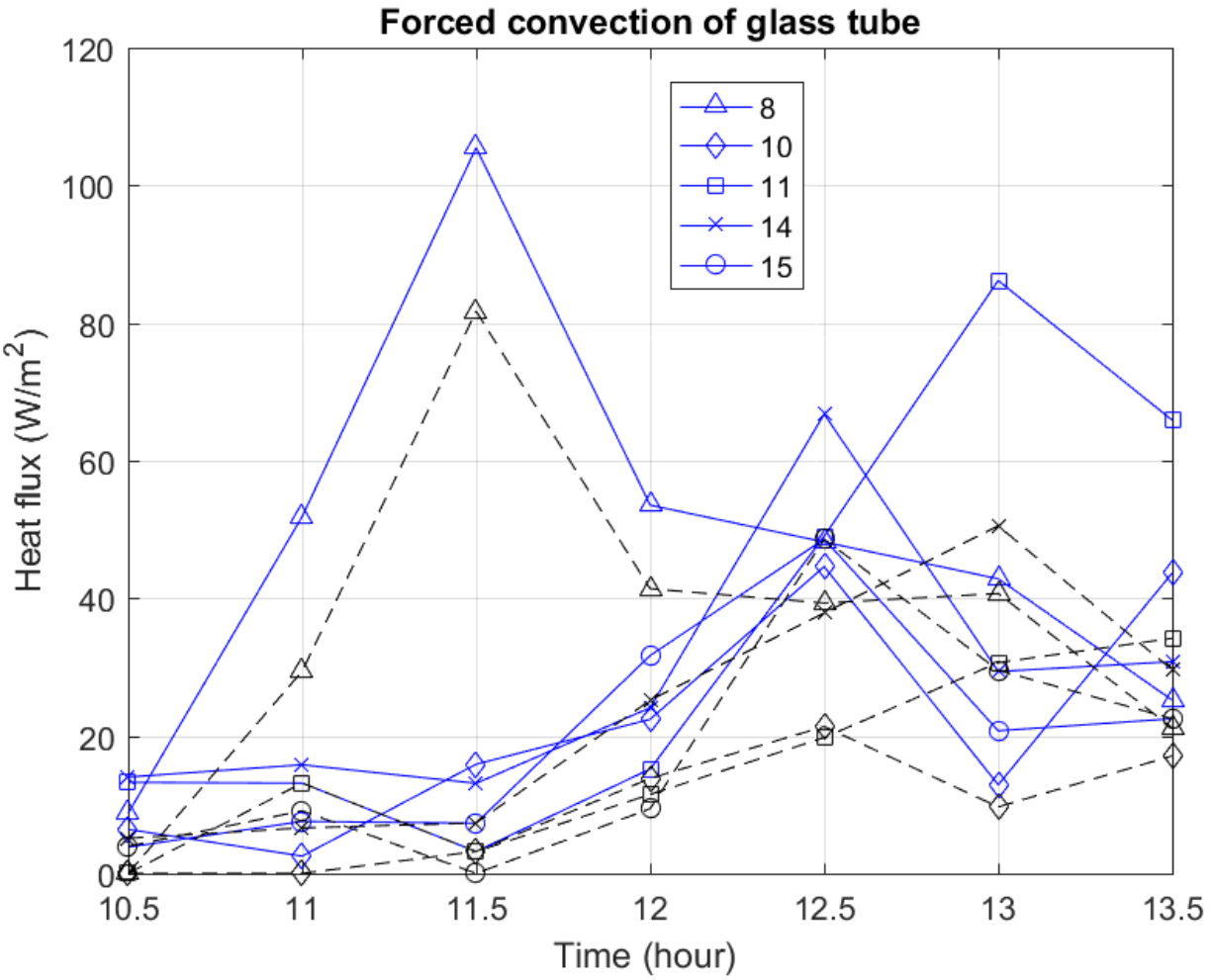

Figure 22: Forced convection Heat flux between glass and environment versus time. solid line are the case without lens and dashed line are the case with lens.

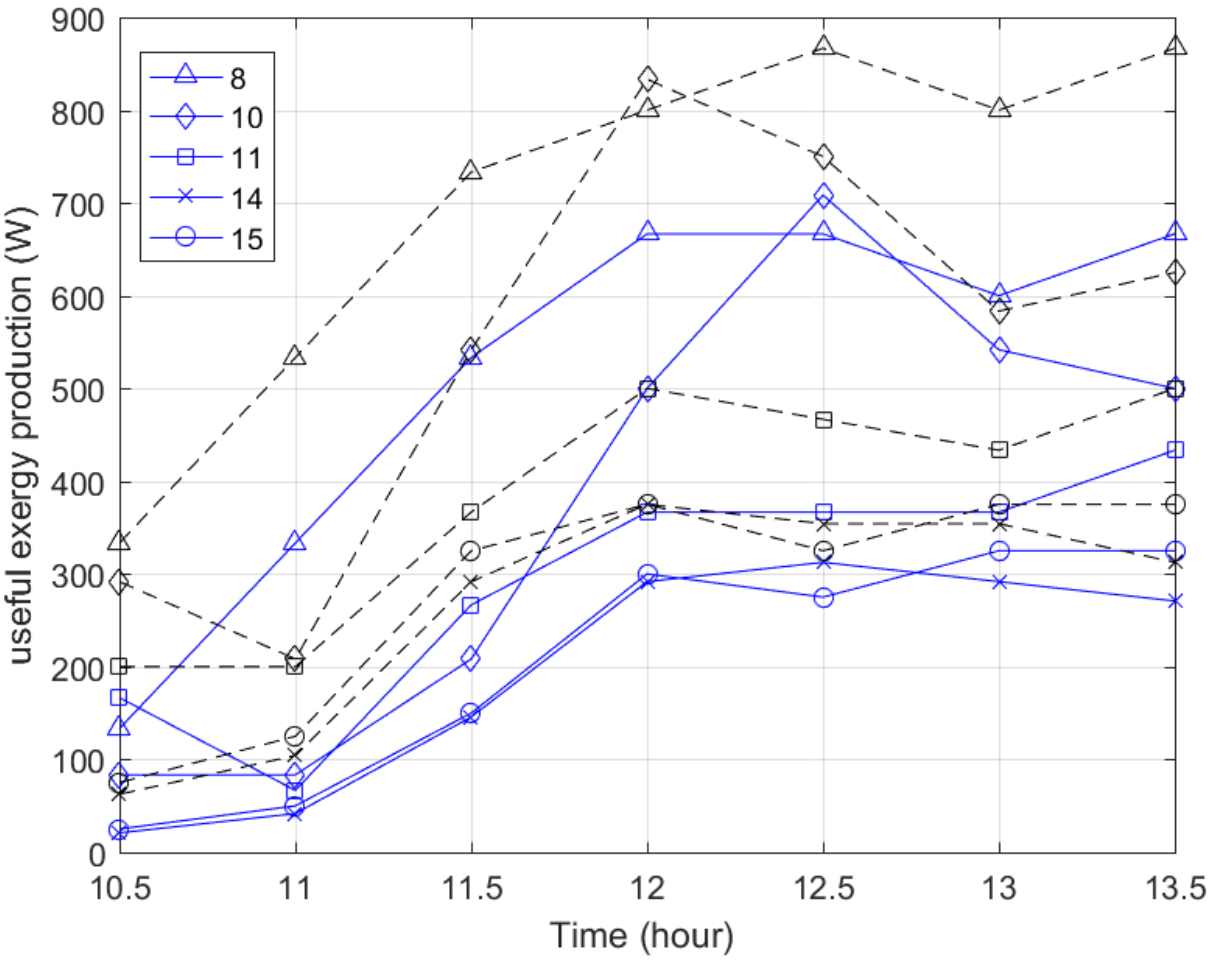

Figure 23: Useful exergy production versus time. solid line are the case without lens and dashed line are the case with lens.

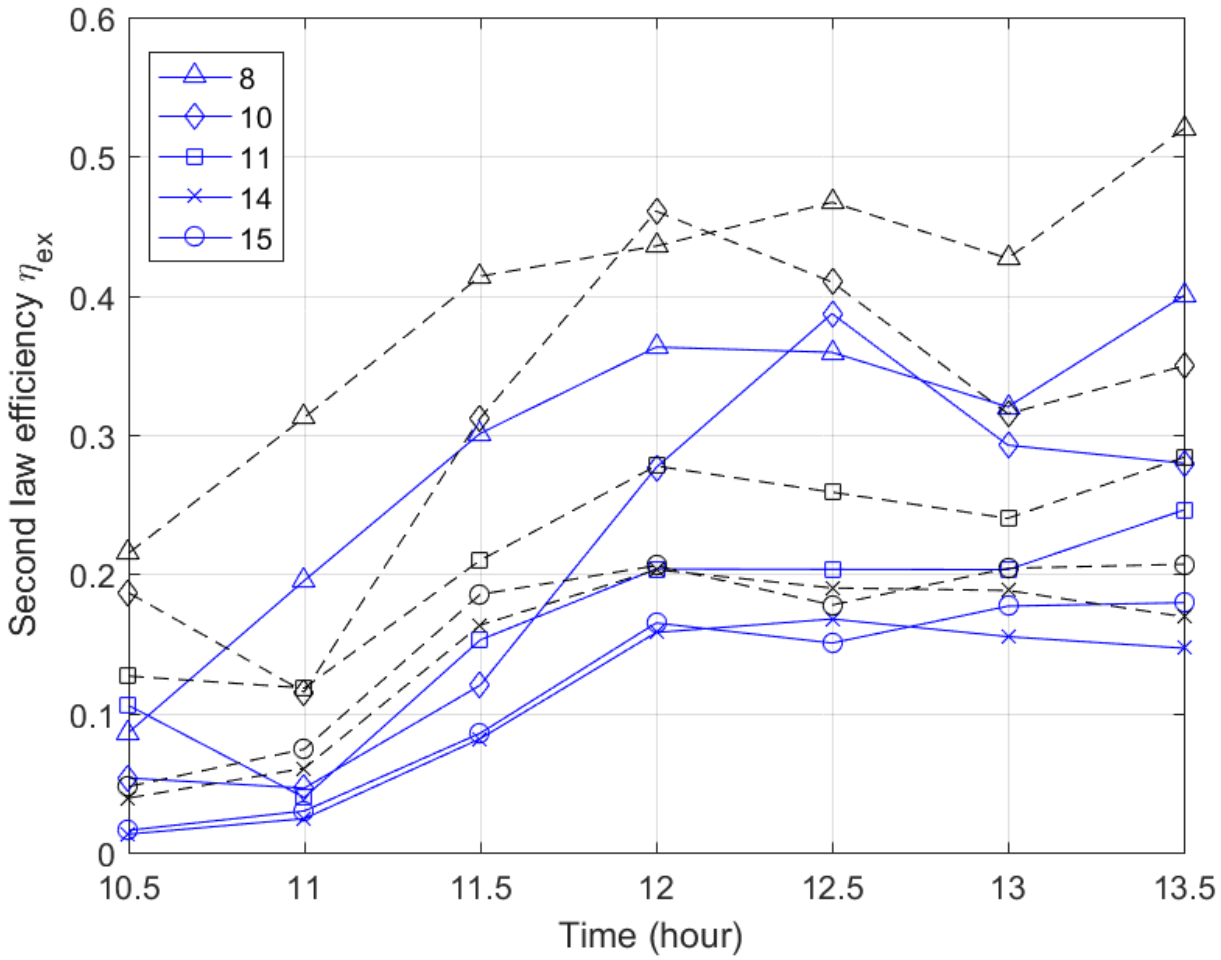

Figure 24: Second law efficiency versus time. solid line are the case without lens and dashed line are the case with lens.